Investigation of electromagnetic interactions by means of electron–photon beams from proton accelerators

B. B. Govorkov

P. N. Lebedev Physics Institute, USSR Academy of Sciences, Moscow
Fiz. Elem. Chastits At. Yadra **11**, 1109–1159 (September–October 1980)

The methods for obtaining electron and photon beams from high-energy proton accelerators are considered. The results of investigations of the electromagnetic interactions of elementary particles obtained by means of these beams are discussed.

PACS numbers: 13.60. – r, 29.25. – t

1. ELECTRON–PHOTON BEAMS FROM PROTON ACCELERATORS

Scheme for Obtaining Electron–Photon Beams. The basic idea for obtaining electron–photon beams from high-energy proton accelerators is due to Markov,[1] who suggested that for this purpose one should use the γ rays from the decay of pseudoscalar mesons $[\pi^0, \eta, \ldots]$. A beam of 70-GeV electrons was obtained for the first time with the Serpukhov proton accelerator.[2]

The basic scheme for obtaining electron and photon beams from proton accelerators is shown in Fig. 1.

When the accelerated protons interact with nuclei, a cone of particles is produced with axis in the direction of motion of the primary particle. The number of particles in the cone increases with the energy; 30–40% of the particles are the neutral mesons $\pi^0, \eta, \ldots$, which decay rapidly ($\sim 10^{-16}$ sec) into photon pairs. Therefore, the first possibility of obtaining a photon beam consists of the direct use of the photons from the decay of the mesons. By means of magnets one can separate the neutral and charged components of the beam. The decay photons have a continuous energy spectrum, which decreases rapidly. Such a beam is called a broad-band photon beam.[3]

Further, if a converter made of a heavy substance is placed in the path of the γ rays, electron–positron pairs are produced, and from these one can obtain electron and positron beams by means of magneto-optical channels. Here, two approaches are adopted. In the first, traditional approach,[1,4,5] the channel separates electrons (or positrons) with given momentum $p \pm \Delta p$; in the second, nonstandard approach, the channel separates electrons with momentum $p \geq p_0$ greater than a given value.[6] It is clear that in the second case of the so-called broad-band electron beam the intensity is much higher.

Finally, one can implement a second possibility for producing photon beams by means of a new radiator (Pb, W, ...). Arranging for coincidence of the bremsstrahlung photon and the electron that emits it, one can produce a system of energy-tagged photons ($E_\gamma = E_{e^0} - E_{e'}$, where E_{e^0} and $E_{e'}$ are the electron energies before and after emission of the photon).[4,7–10] If a crystal (diamond, silicon, etc.) is used instead of an amorphous substance as radiator, it is possible to obtain a beam of tagged linearly polarized photons.[10–14]

The main difficulty in carrying out experiments with all such beams is the large background of μ mesons. We shall now discuss briefly some features of the beams.

Broad-Band γ Beam. A broad-band γ beam was produced for the first time by means of the proton accelerator at Fermilab.[3] The main shortcoming of such a beam is the presence of large admixtures of neutral hadrons $(n, K^0, \ldots)$.

The arrangement at Fermilab is shown in Fig. 2. A beam of protons extracted from the accelerator with energy up to 400 GeV interacts with a beryllium target of thickness 30 cm, producing a beam of neutral particles. A magnet sweeps the charged particles out of the beam. The beam is enriched with photons by the absorption and scattering of hadrons, for which one uses a two-section filter of liquid deuterium of length 34 m, placed in the field of nine magnets, which remove the e^+e^- pairs produced in the deuterium. The coefficient of enrichment is ~200 for 300-GeV initial protons. Of course, the intensity of the photon beam is also reduced by two orders of magnitude. The measured spectrum of the photons that pass through the filter is shown in Fig. 3.[3] The integrated intensity of the photon beam is $\approx 2 \times 10^7$ γ for 10^{12} initial protons (for energies $E_\gamma > 50$ GeV). The broad-band photon beam is convenient for search experiments, in which intensity is more important than a precise value of the photon energy.

As the broad-band beam proposal showed,[11] one can obtain a fairly good intensity for a beam of linearly polarized photons and, possibly, circularly polarized photons by using the method of selective absorption in thick crystals proposed by Cabibbo *et al.*[15] This is because photons with different polarization have different

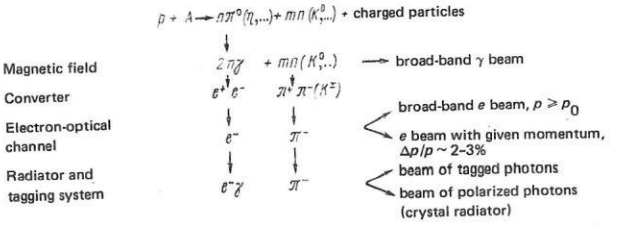

FIG. 1. Scheme for obtaining electron and photon beams in proton accelerators.

 0090-4759/80/050442-20$02.80

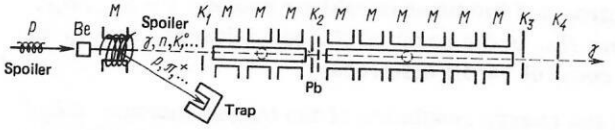

FIG. 2. Arrangement of the Fermilab broad-band γ beam.[3]

cross sections for the production of electron–positron pairs in a crystal structure, so that enrichment occurs when an unpolarized photon beam passes through a crystal, and a beam of photons with distinguished plane of polarization is formed. The efficiency of the thick-crystal method is proportional to the photon energy. According to the estimates of Ref. 11 made for 400-GeV protons with the neutral beam passing through a carbon crystal of thickness 15 cm, the polarization of the photons in the hard part of the spectrum is $P=0.25$, while the beam is attenuated by 5–7 times. For thicker crystals with attenuation by 200 times, $P=0.5$.

Electron Beams with Given Momentum. Beams of electrons with known momentum are more suitable for quantitative measurements. A beam of electrons with given momentum was produced for the first time at Serpukhov.[1] Figure 4 shows the arrangement. It made use of an internal beryllium target, the magnetic field of the accelerator to separate the neutral and charged components of the particles from the target, and the already available electron–optical channel 2 of charged particles as electron channel. This method of obtaining an electron beam was realized in a very short period–six months. The intensities attainable for such beams, the optimal size of the $(\gamma - e^+e^-)$ converter, and the admixture of hadrons $(\pi^-, \ldots)$ were determined for the first time with the Serpukhov accelerator.[1,16] The first physics experiments of this kind were also made with the Serpukhov beam.

Electron beams with given momentum were obtained from extracted proton beams at Batavia and CERN by means of thick beryllium targets (30–40 cm) and special magneto-optical channels.[4,5,8,10]

The parameters of the electron beams obtained from the largest accelerators are given in Table I. It is now possible to obtain high-intensity electron beams with small transverse dimensions (1 cm^2 or less) at the target, small halo of electromagnetic origin ($\sim 10^{-3}$), and

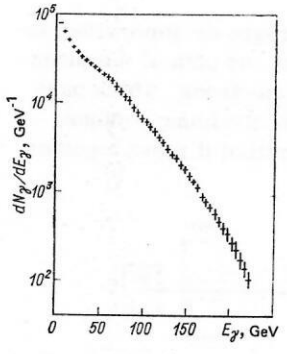

FIG. 3. Spectrum of the photons of the broad-band beam of γ rays produced in a beryllium target by 300-GeV protons.[3] The number of protons incident on the target is 10^{12}.

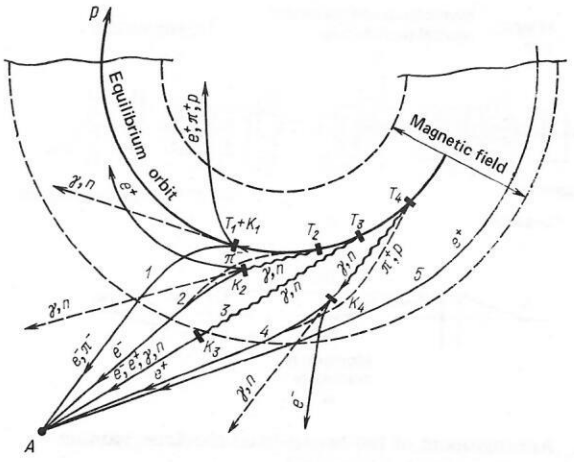

FIG. 4. Methods of generating electron and positron beams at a point in the outer zone of the magnetic ring of the Serpukhov proton accelerator using internal targets. The production angle of the γ rays is $\Theta_\gamma = 0$; $T_i (i=1, \ldots, 4)$ are targets, K_i $(i=1, \ldots, 4)$ are converters, and the paths 1 and 5 are the extreme paths for possible extraction of electrons or positrons to the point A.[1]

low hadron admixture ($\sim 10^{-3}$).

However, the small hadron admixture constitutes an appreciable background because of the difference between the strong and electromagnetic cross sections. Various methods have been proposed to suppress this background: the method of gas Čerenkov counters for beams with low intensity[1]; the use of crystals as converter targets[17]; the use of synchrotron radiation of the electrons in a magnetic field[18–20]; and the use of ondulator radiation of electrons in wigglers.[20] In principle, the last two methods make it possible to separate spatially the electrons and hadrons and reduce the admixture of the latter to 10^{-6}.

Broad-Band Electron Beams. A scheme for obtaining a broad-band electron beam (Broad-Band Electron/Gamma Beam) was proposed in Ref. 6. This is based on the use of a special magneto-optical channel with broad momentum transmission band; all electrons with momentum greater than a given value are transported through the channel. The arrangement of the channel is shown in Fig. 5a and the basic optical scheme in Fig. 5b. Figure 6 shows the calculated spectrum of the broad-band electron beam with lower limit 100 GeV produced by 400-GeV protons. The integrated intensity of electrons with energies 100–300 GeV is 4×10^9 e per pulse

TABLE I. Electron beams from proton accelerators.

Accelerator	Year beam created	E GeV	Target	Angle	Acceptance, μsr	E_e GeV	Flux	Admixture of hadrons, %
Serpukhov[1]	1970	70	Internal, Be, Al	3 mrad	—	35±1.05	$10^6/10^{12}$	0.3
Ref. 27	1978	70	The same	3 mrad	—	40±1.20	$10^6/10^{12}$	—
Fermilab[4]	1974	300	Be:	0	5	115±2.30	$10^7/10^{13}$	0.3–0.4
Ref. 70	1975	400	40.3 cm Be;	0	5	90±1.80	$7 \cdot 10^7/10^{13}$ p	—
Ref. 83	Planned	400	40.3 cm Be;	0	30	200±10.00	$5 \cdot 10^8/10^{13}$ p	10^{-4}
CERN[5,19]	1977	200	40.3 cm —	0	10	80±1.60	$3 \cdot 10^6/10^{12}$ p	10^{-1}
Ref. 6	Planned	400	—	0	—	100–300	$4 \cdot 10^9/10^{13}$ p	—

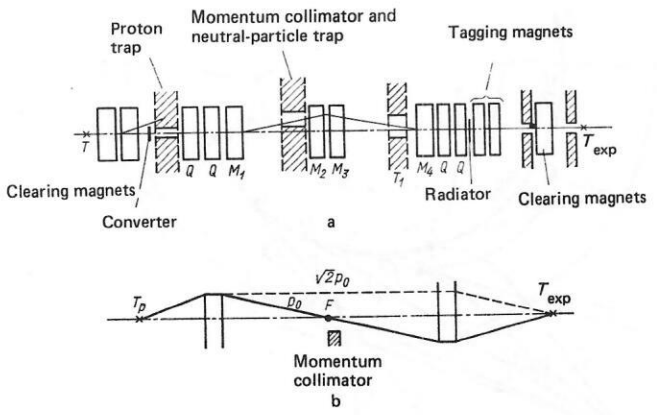

FIG. 5. Arrangement of the broad-band electron/gamma beam (a) and the optical scheme (b).

from 10^{13} 400-GeV protons. The admixture of π mesons in the beam is illustrated by the broken curve in Fig. 6. The muon background at the position of the target is 4×10^{7} μ/m^2. In accordance with the proposal, the momenta of the electrons in the broad-band beam is measured with error 1–2 GeV/c by scintillation hodoscopes placed in the magneto-optical channel.[22] The development of this broad-band beam at CERN opens up new possibilities for the investigation of rare processes.

Beams of Tagged Photons. The tagged-photon method is essentially the missing-energy method applied to the bremsstrahlung reaction $e^0+A\to e'+\gamma+A$. One measures the energy of the electron before, E_{e0}, and after, $E_{e'}$, emission of the photon, so that their difference gives the missing energy carried away by the photon: $E_\gamma=E_{e0}-E_{e'}$.

Multiple processes can be used to increase the γ yield if thick radiators are employed:

$$e^0+A\to e'+\gamma_1+\gamma_2+A;$$
$$e^0+A\to e'+\gamma_1+e^+e^-+A;$$
$$\cdots\cdots\cdots\cdots\cdots$$

In such a case, to determine the energy of the γ_1 it is necessary to measure the energies of all the other photons and electrons. Usually, this is not difficult, since "everything electromagnetic" travels forward.

The tagging system is characterized by the following basic parameters:

a) the efficiency of the correlation between the recoil electron and the bremsstrahlung photon: $\varepsilon=N_{e'\gamma}/N_{e'}$, where $N_{e'\gamma}$ is the count of $e'\gamma$ coincidences, and $N_{e'}$ is the count of recoil electrons;

b) the energy resolution of the tagged photons: $\Delta E_\gamma/E_\gamma=\sqrt{(\Delta E_{e0})^2+(\Delta E_{e'})^2}/E_\gamma$ (as a rule, the energy resolution of the tagging system is determined by the uncertainty ΔE_{e0} in the energy of the primary electron);

c) the agreement between the measured energy of the γ ray and the energy difference $E_{e0}-E_{e'}$.

The possible backgrounds in tagging systems are considered in detail in Ref. 23.

The energy E_{e0} of the primary electron is usually determined by the magneto-optical channel. Tagging systems are usually distinguished by the method employed to measure the energy $E_{e'}$ of the recoil electron.

Magnetic tagging. In this tagging system, the energy $E_{e'}$ is measured by a magnetic spectrometer.[24,25] Such systems are usually used on synchrotrons. An example is provided by the system used on the Serpukhov proton accelerator (see Fig. 13a). The electron beam with momentum 40 ± 1.2 GeV/c formed in the magneto-optical channel strikes the lead radiator R of thickness $0.08X_0$, where X_0 is the radiation length. A magnet is used to determine the momentum of the electrons behind the radiator, a six-channel hodoscope being used to detect the electrons. The hodoscope consists of two separated rows T_1-T_6 and $T_1'-T_6'$ of scintillation counters connected pairwise in coincidence. In this way, recoil electrons with momenta 6–26 GeV are identified, which corresponds to a working interval $E=14$–34 GeV of energies of the tagged photons. The anticoincidence counters A_1-A_4 are used to suppress the background electromagnetic processes.

The photons are detected by the total-absorption spectrometer SD, the pulses from which must be in coincidence with the pulses from the hodoscope of scintillation counters.

The efficiency of the tagging system in this arrangement varied from channel to channel in the range 88–95%.

Pulse-height tagging. In this system, the energy $E_{e'}$ is measured by means of the pulse-height of the pulse from the total absorption spectrometer.[7] The scheme is shown in Fig. 7.

An extended target (liquid hydrogen or some other investigated substance) is placed in the path of the monochromatic beam of high-energy electrons, which pass through the target emitting bremsstrahlung photons. A photon and the electron which emitted it move together

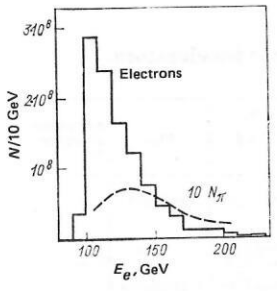

FIG. 6. Spectrum of electrons of the broad-band beam with $E_{\lim}=100$ GeV produced by a beam of 400-GeV protons with intensity $5\times10^{12}p$ (Ref. 6). Interval 10 GeV.

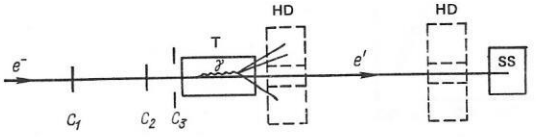

FIG. 7. Pulse-height tagging of bremsstrahlung photons[7]: C_1, C_2, C_3 are scintillation counters, T is the target, HD are hadron detectors, and SS is a shower spectrometer.

through the target [angle $\Theta_{e'\gamma} \approx (mc^2/E_{e0}) \ln(E_{e0}/mc^2)$, where m is the electron mass] in the direction of the initial electron until the photon interacts with one of the target nuclei. The recoil electron passes through the target to the total absorption shower spectrometer (shower Čerenkov spectrometer, scintillation–lead sandwich, etc.). The shower spectrometer serves as the tagging system, the energy of the recoil electron being determined from the pulse-height of the spectrometer.

In this method, the target serves a dual purpose–it is simultaneously the bremsstrahlung radiator and the target for the tagged photons. Therefore, the yield of the investigated reaction depends quadratically on the target thickness.

At high energies (hundreds of GeV or more) pulse-height tagging may be preferable to magnetic tagging on account of its simplicity, high efficiency (100%), and also because the size of the shower spectrometer depends weakly on the energy, $\sim E^{1/3}$, which makes it possible to cover a wide range of γ energies in a single experiment. The system and backgrounds are discussed in more detail in Refs. 7 and 26.

Combined magnetic and pulse-height tagging. In this system, the energy $E_{e'}$ is measured twice–by a magnetic spectrometer and by the pulse-height of a total-absorption spectrometer–which makes it possible to suppress significantly the background processes.

As an example, let us consider the system developed in the Tagged-Photon Laboratory at Fermilab[4,8] (Fig. 8a). Three magnets deflect the recoil electrons into the detecting system, which consists of total-absorption spectrometers and hodoscopes of scintillation counters. Both the electrons and the photons pass through vacuum. To eliminate cases when there is production of pairs in the radiator and δ electrons, an anticoincidence system of counters $A_2, \ldots, A_{11}$ is used. After it has passed through the radiator, the main electron beam is deflected by magnets into a lead and iron trap. The iron serves as a filter, absorbing the muons produced in the trap.

At Fermilab, copper radiators of thickness $0.0053X_0$, $0.0107X_0$, and $0.0266X_0$ were used. For a radiator of thickness equal to 1% of a radiation length, the correction for multiple scattering was 1%. The detecting scheme is shown in more detail in Fig. 8b.

The use of the Čerenkov spectrometers $L_3, \ldots, L_{13}$ made of SF-2 lead glass to detect the electrons led to a measurement of the energy of the particles with higher accuracy than in the magnetic spectrometer and made it possible to suppress the background of pions and muons. The spectrometers L_1 and L_2 were sandwiches made of layers of plastic and lead. The reason for this is that when the integrated dose exceeds 10^9 GeV the SF-2 lead glass begins to color and become opaque. Naturally, the sensitivity and energy resolution of the spectrometer then change. During the working runs, it was necessary to illuminate the glass periodically by a mercury lamp to restore its transparency and to check regularly the energy resolution of the spectrometers. This was done

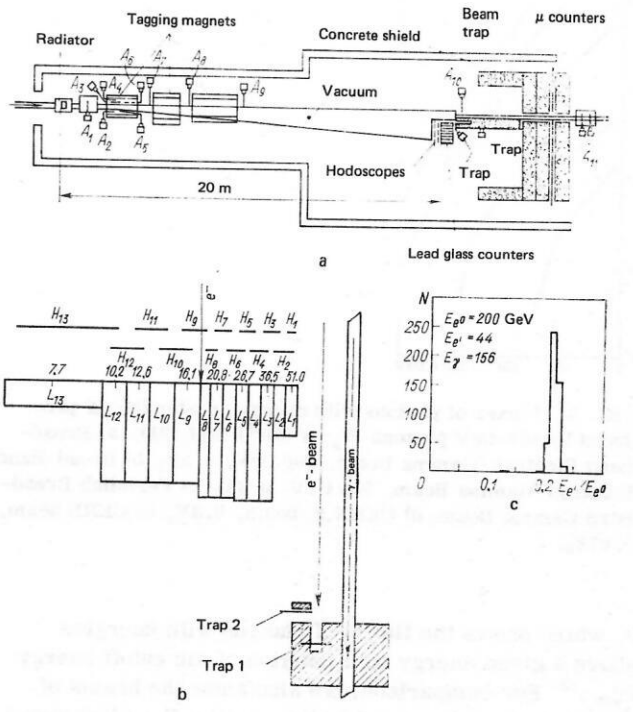

FIG. 8. Combined magnetic and pulse-height tagging of photons at Fermilab[4,8] (a), tagging counters (viewed from above) (b), and spectrum of the tagged photons of the 15th channel for 200-GeV initial electrons (c).

by means of a laser, pulses being sent through thin light tubes to each spectrometer. The operation of the detection system showed that at high counting rates the lead glass total-absorption spectrometers must be replaced by scintillation sandwiches. The numbers above the spectrometers indicate the mean energies of the tagging electrons when the initial electrons have energy 90 GeV.

Ingeniously arranged hodoscopes of scintillation counters (see Fig. 8b) determined the centers of the Čerenkov spectrometers for calibration purposes. Trap 1 was used to absorb the main beam and trap 2 to absorb the electrons which emitted soft photons, which were not used in the experiments.

It can be seen in Fig. 8a that scintillation counters were placed in the muon shield; by connecting these in anticoincidence it was possible to reduce the counting rate of random coincidences with muons by eight times.

This tagging system achieved the truly remarkable $e'\gamma$ correlation of 99.95.

A typical example of the detected range of tagging electrons is shown in Fig. 8c.

Similar tagging systems were developed at CERN[10] and at Serpukhov.[27] A distinctive feature of the CERN system is the use of proportional chambers in both the primary electron channel and the recoil electron detection system. This makes it possible to improve significantly the energy resolution of the system and, which is very important, to use a broad-band electron beam. This then greatly increases the intensity of the beam of tagged photons. The resulting effect can be seen in Fig.

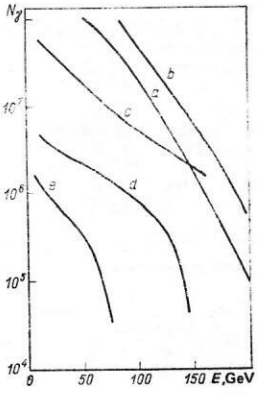

FIG. 9. Fluxes of photons with energy greater than E produced by 400-GeV protons ($N_p = 3\times10^{12}$) (Ref. 21): a) Broad-Band Electron/Gamma Beam, 400 GeV, $0.3X_0$; b) Broad-Band Electron/Gamma Beam, 500 GeV, $0.3X_0$; c) Fermilab Broad-Band Gamma Beam; d) CERN E_4 beam, $0.3X_0$; e) CERN beam, $0.07X_0$.

9, which shows the fluxes of photons with energies above a given energy as a function of the cutoff energy $E_{\gamma\,\mathrm{thr}}$.[22] For comparison, we also show the beams of tagged photons (curves d and e) and the Fermilab broad-band photon beam (curve c).

The creation in proton machines of beams of photons with energy greatly exceeding the energy of classical electron accelerators (linear accelerators and synchrotrons) prepared the way for intensive investigations of electromagnetic interactions of particles in a new energy range, and we now turn to the discussion of these experiments.

2. TOTAL CROSS SECTIONS OF HADRON PHOTOABSORPTION

Total Cross Sections of Hadron Photoabsorption by Nucleons. Photons are fundamental particles, and it is very important to study the interaction of photons with matter. The total cross sections of hadron photoabsorption measure the probability of photon interaction with nucleons. Therefore, measurement of the energy dependence of the total cross section is important for the discovery of new phenomena.

According to modern ideas, the measurement of total cross sections is an important method for studying the hadronic structure of the photon. Hadron-like behavior of photons is predicted by the vector dominance model, in which it is assumed that the photon interacts with hadronic matter like a linear combination of the vector-meson particles ρ, ω, and φ with the quantum numbers of the photon (with spin 1 and negative parity).

In accordance with the model, the total cross section of hadron photoabsorption σ_t can be expressed in terms of the cross sections σ_{VN} for the interaction of the vector mesons with nucleons:

$$\sigma_t = \alpha \sum_V \left(\frac{g_V}{4\pi}\right)^{-1} \sigma_{VN}, \qquad (1)$$

where $\alpha = 1/137$ is the fine structure constant, and $g_V/4\pi$ is the vector-meson–photon coupling constant.

The values of the coupling constants can be determined in independent experiments with colliding beams or from measurement of the dependence of the cross section for the photoproduction of hadrons by nuclei on the mass number (A dependence). The vector-meson–proton cross sections can be determined from the A dependence of the photoproduction of vector mesons or, in accordance with the additive quark model, from data on hadron–proton scattering:

$$\left.\begin{aligned}\sigma_{\rho p} &= \sigma_{\omega p} = (\sigma_{\pi^+ p} + \sigma_{\pi^- p})/2;\\ \sigma_{\varphi p} &= \sigma_{K^+ p} + \sigma_{K^- p} - \sigma_{\pi^- p}.\end{aligned}\right\} \qquad (2)$$

As is shown in Ref. 28, at energies below 20 GeV the vector dominance model describes qualitatively both the value and the energy dependence of the cross section $\sigma_t(\gamma N \to \text{hadrons})$. However, the discrepancy in the absolute values is 10–15%, which was attributed to the inadequacy of taking into account only the ρ, ω, and φ mesons. It was suggested that the discrepancy indicates the existence of new heavier particles with quantum numbers $J^P = 1^-$. Therefore, when beams of high-energy photons were obtained from proton accelerators, one of the first tasks was to measure the total cross sections of hadron photoabsorption by nuclei in the new energy range. In the period 1972–1977, such measurements were made in the energy range 18–185 GeV.[23,30]

The first experiment to measure σ_t on nucleons was made by a P. N. Lebedev Physics Institute–Erevan Physics Institute–Serpukhov Collaboration at Serpukhov.[29]

The experiment used pulse-height tagging of the bremsstrahlung photons. The arrangement of the experiment is shown in Fig. 10a. A beam of electrons with energy 40 GeV (in some runs 31 GeV) was directed onto a target of thickness 1.5 m, which served as both radiator and absorber of the photons. The target consisted of three identical containers of cylindrical shape, one of them filled with liquid hydrogen and another with liquid deuterium, while a third was evacuated and used for background measurements.

The electromagnetic and hadronic processes were distinguished by means of the difference between the angular distributions of these reactions. The secondary particles of the electromagnetic interactions are emitted at small forward angles in the direction of the incident electron, whereas the hadrons are emitted at much larger angles.

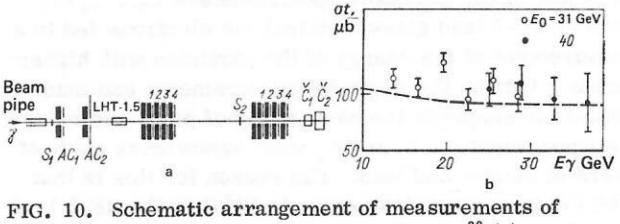

FIG. 10. Schematic arrangement of measurements of $\sigma_t(\gamma p \to \text{hadrons})$ at the Serpukhov accelerator[29] (a); total cross sections for hadron photoabsorption on hydrogen[29] (b). 1–4 are detectors of hadron interactions; S_1 and S_2 are scintillation counters, LHT-1.5 is the liquid-hydrogen target; AC_1 and AC_2 are anticoincidence counters; $\check{C}_1$ and $\check{C}_2$ are total-absorption Čerenkov spectrometers.

The hadron-interaction detectors each consisted of four scintillation counters, between which lead plates of thickness 3 cm were placed. Additional lead absorbers were placed in front of each of these detectors to reduce the detection of soft background electrons and photons emitted at large angles. All the detectors had axial openings with diameter 10 cm to permit the transmission of electromagnetic particles into a composite total-absorption spectrometer ($10X_0 + 12X_0$). The spectrometer measured the energies of the electrons that accompanied the hadronic cases. The intrinsic energy resolution of the spectrometer was 3% (FWHM) for electron energies in the range 26–45 GeV.[29]

Monte Carlo simulation of the electromagnetic processes showed[26] that the contribution of the background processes is appreciably smaller than the effect in the range of photon energies from E_0 to $E_0/2$, where E_0 is the energy of the electrons in the primary beam.

The measured yields of hadronic events were corrected for hadron electroproduction (6–16%), electromagnetic absorption of photons (6.5%), the profile of the bremsstrahlung spectrum (up to 8%), the dead time of the detecting apparatus (10%), and matter in the beam.

The measured values of the total cross sections for hadron photoabsorption by hydrogen and deuterium are given in Fig. 10b and in Table II. It should be noted that because of the uncertainty in the bremsstrahlung spectrum from thick targets the systematic error in the values of the cross sections is 10–15%.

Measurements of $\sigma_t(\gamma p \to \text{hadrons})$ of significantly higher accuracy and in a wider energy range were made at Batavia in the Fermilab Tagged-Photon Laboratory by a Santa Barbara–Toronto–Fermilab Collaboration led by Caldwell.[30] Combined magnetic and pulse-height photon tagging was used. The cross sections on hydrogen were measured to an accuracy of fractions of a percent at energies from 18 to 185 GeV. A method was employed in which all hadrons produced by photons in a liquid-hydrogen target of length 1.00027 ± 0.00025 m were counted. Data were obtained at different energies of the primary electrons $E_0 = 40$, 60, 90, 135, and 200 GeV, and the interval of photon energies E_γ for each E_0 was divided into six parts.

TABLE II. Total cross sections for hadron photoabsorption (μb) (Ref. 29).

Momentum 31 GeV/c of the beam electrons						
E_γ, GeV	13.5	16.5	19.5	22.5	25.5	28.5
$\sigma_t(\gamma p)$	110±5	105±5	119±5	98±6	109±7	100±8
$\sigma_t(\gamma d)$	195±9	209±10	203±12	205±13	189±15	195±17
$\sigma_t(\gamma n)$	91±10	110±11	90±13	113±14	86±16	100±19
Momentum 40 GeV/c of the beam electrons						
E_γ, GeV	24.8±2		28.8±2	32.8±2		36±2
$\sigma_t(\gamma p)$	104±9		108±10	99±12		97±17

The arrangement of the apparatus in this experiment is shown in Fig. 11. The hadrons produced in the 1-m long liquid-hydrogen target were detected in the three detectors $H1$, $H2$, and $H3$, each of which detected π^0, p, and π^+ with high efficiency. Neutrons and K mesons were detected with ≈90% efficiency in the Pb-Fe scintillator sandwich $S3$. The total absorption spectrometer C measured the energy of the photons that had not interacted in the target and the greater part of the e^+e^- pairs. The low-energy electrons that did not reach C as well as the other electromagnetic channels were identified by the block of proportional chambers PC and the hodoscope $G3$ of total-absorption spectrometers. The central hadrometer and sandwich of Fe and liquid scintillator, which were placed at the end of the facility, were used to identify cases of production of hadrons by photons in the spectrometer C and to detect hadrons which had passed through the axial openings in the hadron detectors $H1$, $H2$, $G3$, and $S3$.

The systematic error of the results was estimated at 0.7%, but its energy-dependent part was ≈0.4%.

The measured values of $\sigma_t(\gamma p \to \text{hadrons})$ are given in Table III and in Fig. 12. Representation of the results for $E_\gamma > 35$ GeV by an $a + bE_\gamma$ dependence led to the expression

$$\sigma_t = (112.76 \pm 0.41) + (0.0272 \pm 0.0050)\, E_\gamma,$$

which indicates a growth of the cross section at energies $E_\gamma > 35$ GeV.

Comparison with the predictions of the simplest form of the vector dominance model (allowance for ρ, ω, and ϕ in accordance with Refs. 1 and 2) showed that this model describes neither the magnitude nor the energy dependence of the cross section. The curves are normalized to the experimental results at energies below 16 GeV.

Better agreement is achieved with a phenomenological model which generalizes the vector dominance model by taking into account the contributions of heavier vector mesons, in particular, charmed mesons.

In this model, one specifies[31]:

a) the mass spectrum of the vector mesons. For the distances between the levels of the ordinary quark–antiquark states (u, d, and s quarks and the families of ρ, ω, and ϕ mesons) one takes the form

$$N = C\,(M_N^2 - M_0^2)/2, \quad N = 0,\ 1,\ 2,\ \ldots,$$

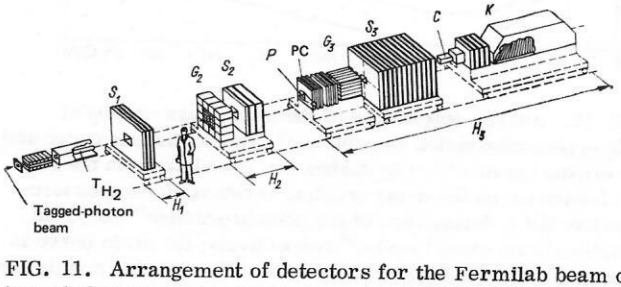

FIG. 11. Arrangement of detectors for the Fermilab beam of tagged photons used in measurements of the total cross sections for photoabsorption.[30]

TABLE III. Total cross sections for hadron photoabsorption on hydrogen.[30]

E_0, GeV	E_γ, Gev	σ_t, μb	$\Delta\sigma_t$, μb
40	18.3	116.91	0.70
	23.2	115.37	0.74
	27.7	113.74	1.03
	30.9	114.34	1.09
	34.2	114.84	1.10
	36.5	112.18	1.41
60	31.4	114.19	0.55
	37.9	113.50	0.60
	43.9	114.57	0.83
	48.4	114.57	0.87
	52.6	114.25	0.88
	55.6	114.06	1.14
90	44.5	114.84	0.50
	54.9	113.11	0.54
	64.3	114.81	0.76
	71.4	114.00	0.79
	77.9	114.09	0.79
	82.4	116.61	1.02
135	67.9	114.58	0.56
	83.9	115.89	0.61
	98.6	115.59	0.89
	109.1	113.82	0.89
	118.8	116.52	0.99
	126.0	114.30	1.13
200	98.9	115.85	0.74
	121.8	116.37	0.87
	142.0	115.80	1.31
	157.8	119.78	1.30
	172.2	116.37	1.34
	182.7	118.49	1.62

where C is a constant characteristic of each family, and M_N is the mass of the N-th vector meson. For the J/ψ family, $N = C(M_N^3 - M_\psi^3)/2$;

b) the cross sections for the interactions of the vector mesons with the nucleons. It is assumed that all mesons consisting of identical quarks have equal total cross sections for interaction with nucleons;

c) the vector-meson–photon coupling constants. The recursion relation for the coupling constants have the form

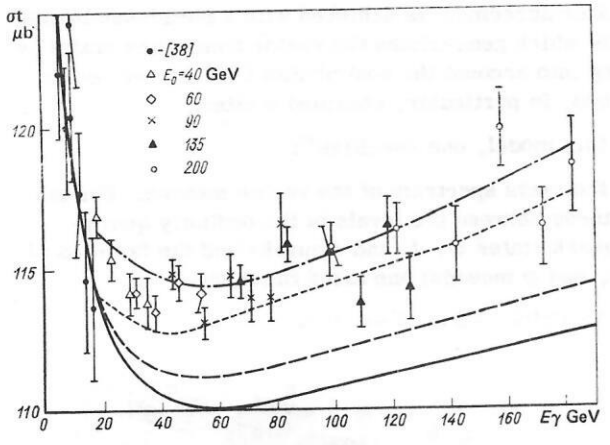

FIG. 12. Energy dependence of the total cross section of hadron photoabsorption on protons.[30] The continuous curve and the broken curve with long dashes are calculations in the vector dominance model using coupling constants from measurements of the A dependence of the photoproduction[28] and from colliding-beam experiments,[28] respectively; the chain curve is calculated in accordance with the generalized vector dominance model; the broken curve with short dashes, in accordance with the quark model.

$(g_V^2/4\pi)(M_V) = (g_V^2/4\pi)(M_0)(M_V/M_0)^3$ for the ρ, ω, and ϕ families;

$(g_V^2/4\pi)(M_V) = (g_V^2/4\pi)(M_0)(M_V/M_0)^4$ for the J/ψ family.

The total cross section for hadron photoabsorption calculated under these assumptions without any normalizations is shown by the chain curve in Fig. 12.

Another model, which gives a reasonable description of the data of Ref. 30, is the quark model, according to which the photon is directly coupled to quark–antiquark pairs, with, moreover, strength proportional to the charge of the quark:

$$\gamma \sim (2/3)\, u\bar{u} - (1/3)\, d\bar{d} - (1/3)\, s\bar{s} + (2/3)\, c\bar{c};$$

accordingly, the total cross sections are related to the total cross sections of quark–hadron interactions[30]:

$$\sigma_{\gamma p} \sim (2/3)^2 \sigma_{u\bar{u},\, p} + (-1/3)^2 \sigma_{d\bar{d},\, p} + (-1/3)^2 \sigma_{s\bar{s},\, p} + (2/3)^2 \sigma_{c\bar{c},\, p}.$$

The broken curve in Fig. 12 is calculated in this model. The quark–hadron cross sections were calculated using the data of hadron–hadron scattering. This curve is normalized to the data at $E_\gamma \leq 16$ GeV.

The main conclusion drawn in Ref. 30 is that the total cross sections of hadron photoabsorption were measured with error less than 1%. In the energy range 18–185 GeV, a 4% growth in the cross section is observed. This growth is stronger than the similar growth in the hadron–hadron cross sections, which may be regarded as an indication of a large contribution of charmed quarks to the total cross section and a possible strong coupling of the photon to charmed quarks. This makes a high-energy photon beam an excellent tool for investigating charmed mesons and charmed baryons.[30]

Total Cross Sections of Hadron Photoabsorption by Nuclei. The study of the toal cross sections of hadron photoabsorption by nuclei is important for investigating screening effects.[32–34] The screening effect is as follows: If a hadronic component of the photon exists at a sufficiently large distance from the point of interaction of the photon within the nucleus, the nucleus will exhibit a tendency to screening. It is of interest to study this phenomenon experimentally, since it provides direct proof of the hadronic structure of the photon.

The screening effect is most clearly manifested in different nuclei in terms of an effective nucleon number given by

$$A_{\text{eff}}/A = \sigma_{\gamma A}/[Z\sigma_{\gamma p} + (A - Z)\,\sigma_{\gamma n}],$$

where Z is the number of protons in the nucleus with mass number A.

The first measurements of the total cross sections of hadron photoabsorption by carbon nuclei in the new energy range $E_\gamma > 20$ GeV were made by a Erevan–Serpukhov group in 1975.[35] They used the magnetic tagging system described earlier. Figure 13a shows the arrangement of the experiment. Hadron photoabsorption events were detected by lead–scintillation sandwiches. Hadronic events were determined by coincidences of $(H_1H_2H_3H_4)$ or $(H_1H_2H_5H_6)$ with a signal from the tagging system in the absence of a pulse in the spectrometer SD.

The measured yields were corrected for absorption

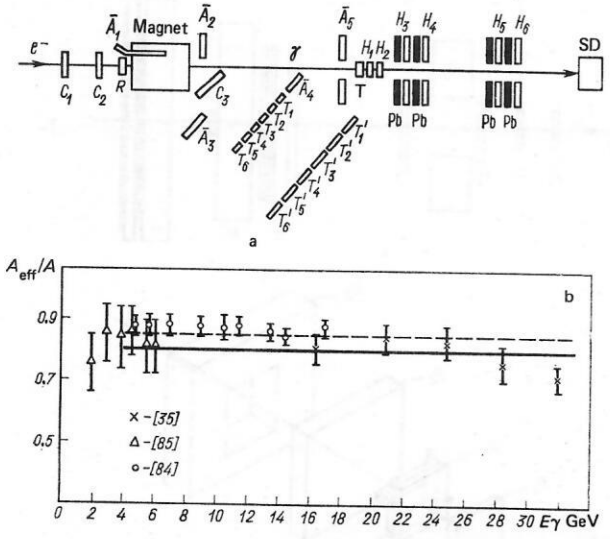

FIG. 13. Arrangement of experiment to measure total cross sections of hadron photoabsorption on carbon nuclei[35] (a) and energy dependence of the ratio A_{eff}/A for the carbon nuclei (b). C_i are scintillation counters, R is the radiator, T_i and T_i' are target scintillation counters, A_i are anticoincidence counters, T is the carbon target, H_1–H_6 are the detectors of hadron interactions, and SD is the total-absorption spectrometer.

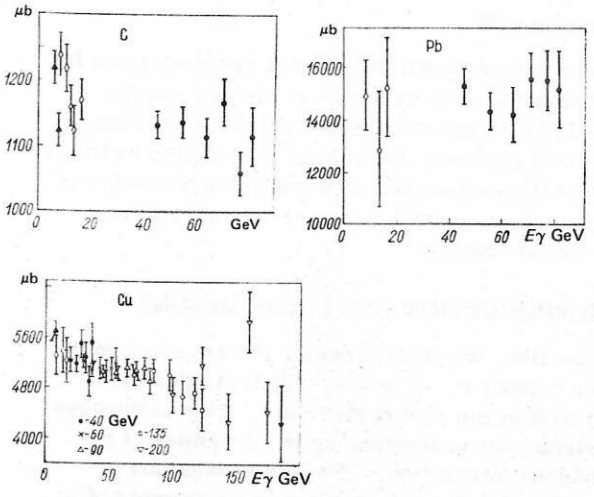

FIG. 14. Total cross sections for hadron photoabsorption by carbon, copper, and lead nuclei.[36] The black triangles are the data of Ref. 86, the open diamonds the data of Ref. 84, and the crosses, open triangles, open circles, and open inverted triangles are the data of Ref. 36.

of the photon beam, attenuation of the beam due to misalignment of its section with the area of the target (5%), the count of random coincidences (1%), the count in the absence of a target (5–14%), the count of multiple bremsstrahlung processes (10–15%), the electromagnetic background (2%), the geometrical losses of ρ mesons (0.5–1.5%), and the efficiency of the hadron detectors.

The measured values of the total cross sections $\sigma_t(\gamma C \to \text{hadrons})$ are given in Table IV. Figure 13b shows A_{eff}/A as a function of the energy. The decrease in the energy range 27–34 GeV was attributed by the authors in part to the circumstance that the contribution of the purely neutral photoproduction channels was not detected in the experiment.

More accurate and complete measurements of the screening effect were made at Batavia by the Santa Barbara–Toronto–Fermilab group.[36] They used the apparatus employed to measure the total cross sections on hydrogen described earlier. Carbon, copper, and lead targets were used. Their thickness was $0.1X_0$. For calibration, the cross sections for the photoproduction of electron–positron pairs were measured; to within 2%, these were equal to the cross sections calculated by Tsai.[37] Special experiments tested the possible geometrical losses of hadron events and a possible dependence of the results on the thickness of the tagging-system radiator. It was shown that with an error 2% these corrections are unimportant.

TABLE IV. Total cross sections for hadron photoabsorption on carbon nuclei.[35]

E_γ, GeV	14—19	19—23	23—27	27—30	30—34
σ_t (γC), μb	1082±56	1105±50.5	1080±57	980±67.7	930±44

In the measurements with carbon, copper, and lead targets the energy of the initial electrons was $E_0 = 90$ GeV; with the copper target, measurements were also made at $E_0 = 40$, 60, 135, and 200 GeV. The energy range of the tagged photons was $[0.5E_0, 0.91E_0]$. The approximate systematic errors were $^{+1.3}_{-0.8}$% for the carbon and copper targets, and $^{+2.4}_{-1.1}$% for the lead.

The measured values of the total cross sections on carbon, copper, and lead nuclei are given in Fig. 14, in which we have also plotted data obtained at lower energies.

In the calculation of A_{eff}/A, use was made of an approximation of the data for a hydrogen target[30]: $\sigma_{\gamma p} = A + B\ln E_\gamma + C\sqrt{E_\gamma}$; $\sigma_{\gamma n}$ was calculated from the approximation of the difference measured at low energies[38]: $\sigma_{\gamma p} - \sigma_{\gamma n} = (18.3 \pm 6.1)/\sqrt{E_\gamma}$ μb (E_γ is measured in GeV). The obtained values of the screening parameter are given in Fig. 15. The data for copper reveal an increase in the screening with increasing energy. The vector dominance model does not predict such behavior. Caldwell *et al.*[36] draw attention to the possibility of describing the data by taking into account the nondiagonal terms in the vector dominance model,[28,36] which corresponds to the "inelastic scattering" of the forward scat-

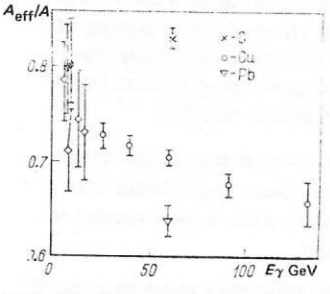

FIG. 15. Energy dependence of A_{eff}/A.[36]

tering amplitude.[39]

Thus, the measurement of the total cross sections for hadron photoabsorption by nuclei in the new energy range 20–185 GeV not only reconfirmed the screening effect for real photons, illustrating thereby the hadronic structure of the photon, but also led to the discovery of a new phenomenon–growth in the screening with increasing photon energy.

3. PHOTOPRODUCTION OF VECTOR MESONS

In this section, we shall consider photoproduction of the vector mesons ρ, ω, and ϕ, which provide the dominant part of the photon structure. This is because it is important for understanding the dynamics of the photon–hadron interaction. The photoproduction $\gamma + N(A) \to V + N(A)$ of vector mesons is an example of a diffraction process. In accordance with the vector dominance model, the photoproduction of V is equivalent to diffraction of vector mesons and, therefore, is similar to hadronic processes at high energies. It is important to test the analogy between photons and hadrons at even higher energies.

The investigation of the photoproduction of vector mesons by nuclei is a source of fundamental information about the total cross sections σ_{VN} for the interaction of vector mesons with nucleons and the vector-meson–photon coupling constants $g_V/4\pi$.

The first measurements of the photoproduction of vector mesons in the new energy range were made at Batavia with the broad-band photon beam.[3] An extracted beam of 300-GeV protons and a baryllium target were used. The schematic arrangement of the experiments is shown in Fig. 16. The detector consisted of a magnetic spectrometer with multiwire proportional chambers P_0, P_1, P_2, P_3, P_4 and an identifier of the particles e, H, and μ. The scintillation detectors T, AB, and AW (see Fig. 16b) covered the regions missed by the proportional chambers. The counters T were used to detect the recoil protons, while the counters AB and AW covered the forward peak.

The particle identifier consisted of an electron–photon calorimeter, a hadron calorimeter, and a muon identifier. The electron–photon calorimeter consisted of two parts (Fig. 17). The first part contained six layers of lead and six layers of scintillator, and the second 16 layers of the one and the other.

The hadron calorimeter consisted of 24 steel plates, each of thickness 4.45 cm, interlaid with 6.3-mm strips of plastic scintillator. A square opening of side 15 cm in the center of the calorimeter allowed the passage of the beam. The muon identifier consisted of steel absorbers and scintillation hodoscopes; the vertical hodoscope had 18 elements, the horizontal one 22.

The intensity of the photon beam was measured by a Wilson quantometer ($26X_0$). The photon spectrum was determined in special experiments with a lead target of thickness $0.04X_0$ using e^+e^- pairs.

In the working runs, magnetic tape was used to record events with the detection of two or more electrons, two

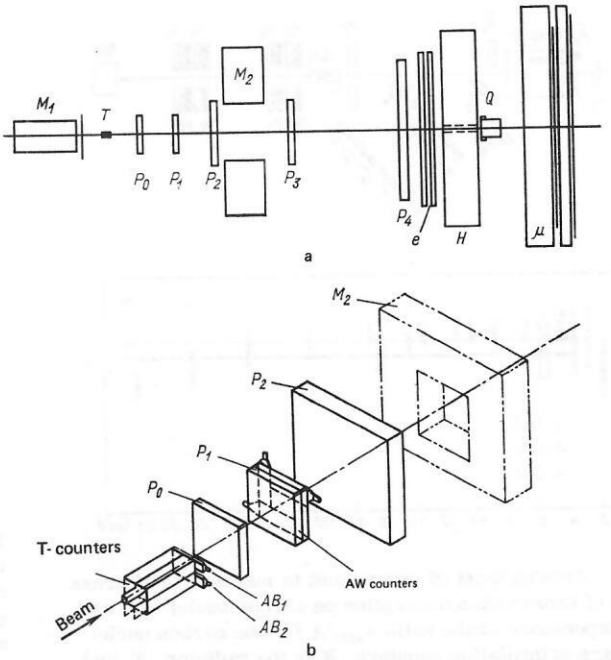

FIG. 16. Arrangement of experiment with the Fermilab broad-band beam (a) and the scintillation detectors (b) (Ref. 3). M_1 is the clearing magnet, T is the target, P_0—P_4 are proportional chambers, M_1 and M_2 are magnetic spectrometers, Q is a Wilson quantometer, and e, H, and μ are electron, hadron, and muon detectors.

or more muons, one electron and one muon, and also events in which an appreciable fraction of the energy was deposited in the hadron calorimeter. For each event all tracks were reconstructed from the data of the proportional chambers.

In the study of the reaction

$$\gamma + \mathrm{Be} \to V + \mathrm{Be},$$
$$\qquad\quad \hookrightarrow \mathrm{Hadrons}$$

where V are the diffraction-produced hadronic particles, events without particles in the counters AB and AW with the absence of π^0 mesons were selected. The mass spectra and distributions with respect to the square of the momentum transfer t were calculated under the assumption that all the observed particles were charged pions. The t dependence for two-particle states is shown in Fig. 18. The mass spectra for two and four charged particles in the final state for $-t < 0.025$ $(\mathrm{GeV}/c)^2$ are given in Fig. 19 with allowance for

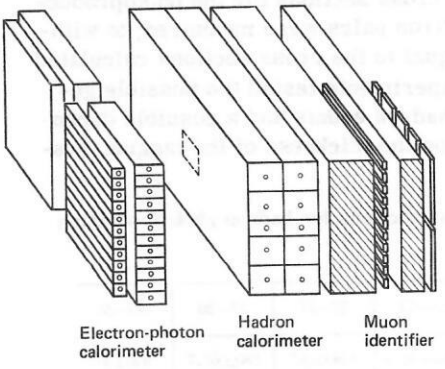

FIG. 17. Particle identifier.[3]

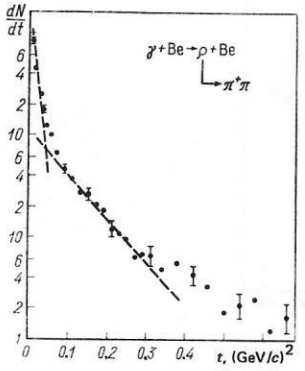

FIG. 18. The t distribution of ρ mesons in the case of photoproduction on a beryllium target initiated by the Fermilab broad-band γ beam.[3]

the acceptance. Peaks are clearly observed for $\rho \to \pi^+\pi^-$, $\rho'' \to \pi^+\pi^-$ and $\rho'' \to \pi^+\pi^-\pi^+\pi^-$. If it is assumed[28] that the complete 4π peak is due to the $\rho''(1600)$ meson, then, $\Gamma(\rho'' \to \pi^+\pi^-)/\Gamma(\rho'' \to \pi^+\pi^-\pi^+\pi^-) \approx 5\%$.

In the mass spectrum for 6π a peak is observed at $M = 2.2$ GeV, but it is assumed in Ref. 3 that the statistical accuracy of the results is inadequate for definite conclusions.

The same group reported new data on photoproduction of ρ'' mesons at the 1979 International Symposium on Lepton and Photon Interactions at High Energies.[40]

At the medium photon energies 75 and 135 GeV, they studied the reactions $\gamma p \to \pi^+\pi^- p$, $\gamma C \to \pi^+\pi^- C$, and $\gamma C \to \pi^+\pi^-\pi^+\pi^- C$. In the mass spectrum of the 2π system, they observed a peak at $M_{\pi\pi} = 1600 \pm 10$ MeV with width $\Gamma = 283 \pm 10$ MeV. The cross section for the production of this particle is approximately 160 nb. In the mass spectrum of the 4π system, a peak is also observed at $M_{4\pi} = 1.6$ GeV, but with a width twice that for the 2π system.

First results on the photoproduction of ρ^0 and ϕ mesons were reported by Caldwell *et al.* at the Tokyo Conference (Toronto–Santa Barbara–Fermilab Collaboration).[41,42]

From the data recorded on magnetic tape during measurement of the total cross sections of hadron photoabsorption (see Sec. 2) two-particle events were selected. The product of the angle between the two particles and their energy, which was assumed to be equal to the energy of the tagged photon, was taken as equivalent to the invariant mass. The separation Δ of the two tracks (the distance between the coordinates of the points of entrance of the particles into the detector) for decay $M \to 2m$ at energy E is determined to good accuracy by

$$\Delta = \frac{4z \sin\Theta \sqrt{(M/2)^2 - m^2}}{E\{\sin^2\Theta + (2m/M)^2\cos^2\Theta\}},$$

where Θ is the decay angle in the M rest system, and z is the distance from the target to the detector at which Δ is measured.

For the decay $\phi \to K^+K^-$, the maximal separation of the tracks was $\Delta_M\phi = 0.509z/E$, whereas almost all decays of ρ mesons led to $\Delta \geq 1.432z/E$ ($\theta = 90°$). The product $E\Delta$ or the ratio $R = \Delta/\Delta_M\phi$ does not depend on the energy, which makes it possible to represent the R spectrum for the complete tagging interval. Cases in which 35% of the energy of tagged photon was deposited in the detector $H3$ were included in the spectrum. The detectors $S1$, $S2$, and $G2$ served as veto counters. An example of the R spectrum for $E_0 = 90$ GeV is shown in Fig. 20. One can clearly see the peaks of the ρ and ϕ mesons.

Monte Carlo calculations were made to determine the yields of ρ^0 and ϕ mesons. The program took into account the photon spectrum, the mass spectrum of the ρ^0 mesons, the geometrical acceptance, the target length, the beam diameter, and the energy resolution. Conservation of the s-channel helicity in the investigated processes and an exponential form of the t distribution were assumed. Allowance was also made for the contributions from the process $\phi \to K_2^0K_s^0 \to K_2^0\pi^+\pi^-$ and the background of e^+e^- pairs, which are shown in Fig. 21.

The yields of ρ^0 and ϕ mesons were corrected for the

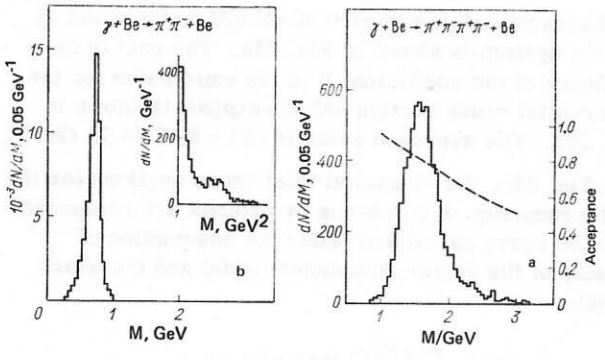

FIG. 19. Photoproduction mass spectra of the final states for two (a) and four (b) pions.[3] The broken curve shows the detector acceptance for the phase space of the final states.

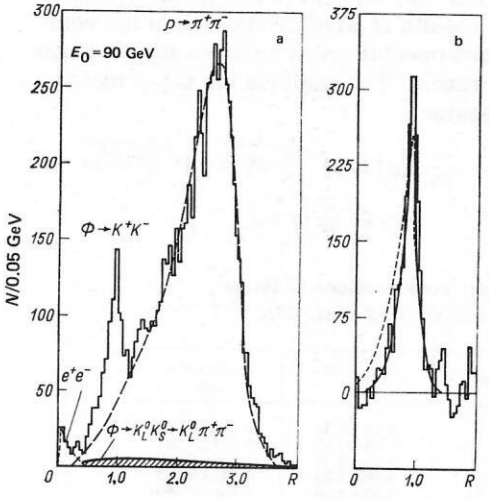

FIG. 20. The R spectrum for the photoproduction of pairs of charged particles at electron energy $E_0 = 90$ GeV (a) and of ϕ mesons (b) obtained from (a) by subtraction of the ρ mesons and e^+e^- pairs.[42] The broken curves with long and short dashes show the contribution of ρ mesons (a) and ϕ mesons (b) calculated by the Monte Carlo method.

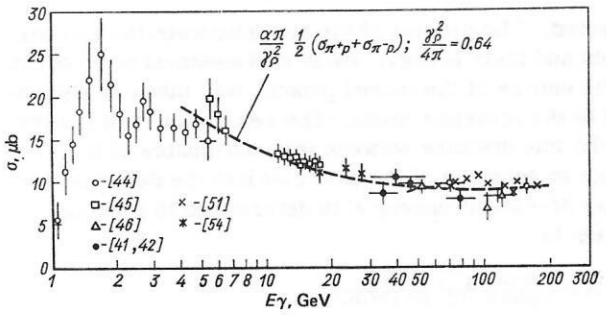

FIG. 21. Energy dependence of the total cross section of ρ^0-meson photoproduction on protons.

acceptance (60% for ρ and 96% for ϕ), the inefficiency of two-track detection in the chambers (9%), inelastic interactions with the material of the chambers, decay in flight, and inelastic events due to target dissociation (13 and 18%). The last correction was determined experimentally from data obtained with recoil counters that surrounded the target.

The measured total cross sections for photoproduction of ρ^0 and ϕ mesons are shown in Table V and in Figs. 21 and 22a together with the results of previous measurements.[43-49] The results for ρ^0 mesons are compared with the theoretical curve calculated under the assumption of validity of the vector dominance model and the additive quark model. Under these assumptions,

$$\frac{d\sigma}{dt}(\gamma p \to \rho^0 p) = \frac{e^2}{4\gamma_\rho^2}\left[\frac{p_\pi^*}{2p_\gamma^*}\left\{\sqrt{\frac{d\sigma}{dt}(\pi^+ p)} + \sqrt{\frac{d\sigma}{dt}(\pi^- p)}\right\}\right]^2, \quad (4)$$

where p_π^* and p_γ^* are the momenta of the π and the γ in the πp and γp center-of-mass systems. All the estimates are for equal values of s.

Integration of (4) leads to the expression

$$\sigma(\gamma p \to \rho^0 p) \approx \frac{e^2}{4\gamma_\rho^2}\frac{1}{2}[\sigma(\pi^+ p \to \pi^+ p) + \sigma(\pi^- p \to \pi^- p)],$$

which was calculated for the coupling-constant value $\gamma_\rho^2/4\pi = 0.64$ (Ref. 50) (the curve in Fig. 21). Figure 22a shows the results of parametrization of the complete set of experimental cross sections for photoproduction of ϕ mesons. The analysis for the ϕ meson used the expression

$$\frac{d\sigma}{dt}(\gamma p \to \phi p) = \frac{e^2}{4\gamma_\phi^2}\frac{1}{(p_\gamma^*)^2}\left[p_k^*\left(\sqrt{\frac{d\sigma}{dt}(K^+ p)} + \sqrt{\frac{d\sigma}{dt}(K^- p)}\right) - p_\pi^*\sqrt{\frac{d\sigma}{dt}(\pi^- p)}\right]^2,$$

TABLE V. Total cross sections of the processes $\gamma p \to \rho^0 p$ and $\gamma p \to \phi p$ (Ref. 42).

E_0, GeV	$E\gamma$ GeV	$\sigma_{\gamma\to\rho} \pm \Delta\sigma$, μb	$\sigma_{\gamma\to\theta} \pm \Delta\sigma$, μb
60	35±5	8.84±0.44	0.506±0.090
60*	42±12	10.68±0.67	0.568±0.091
60	47±7	9.90±0.49	0.546±0.089
90	53±7	9.50±0.56	0.625±0.063
90	71±11	9.82±0.56	0.646±0.065
135	79±11	8.24±0.47	0.648±0.052
135	106±16	9.22±0.52	0.661±0.053
200	117±17	8.59±0.49	0.630±0.101
200	157±23	9.75±0.56	0.740±0.092

*Data obtained with changed geometry of the experiment.

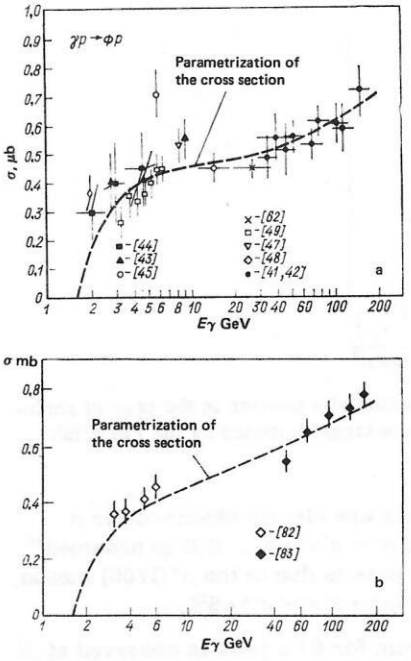

FIG. 22. Total cross sections for photoproductions of ϕ mesons on protons (a) and the cross sections calculated in the vector dominance model and the quark model and normalized to the experimental data for ϕ mesons (b).

the data on forward scattering, and an exponential profile of the t distribution [$b(s) = 4.66 \pm 0.38 \ln s$].[42] The obtained curve, normalized to the experimental data, is shown in Fig. 22b. The value of the coupling constant was determined from the normalization conditions of the two curves: $\gamma_\phi^2/4\pi = 4.7 \pm 0.3$.

It is concluded in Ref. 40 that the energy dependence of the elastic ϕp cross section from the hadron data (in accordance with the quark model) agrees with the dependence from the photoproduction (in accordance with the vector dominance model).

Experimental data on the photoproduction of ω mesons by protons were obtained for the first time by the same group and reported at the 1979 Batavia Symposium.[51]

The ω mesons were detected through the decay mode $\omega \to \pi^0\gamma$, the property of 2π overlapping by the γ spectrometers being exploited to select 3γ events. The 2γ mass spectrum was restricted to the interval 80–200 MeV.

The measured dependence of dN/dM on the mass of the $\pi^0\gamma$ system is shown in Fig. 23a. The energy dependence of the coefficient B in the expression for the differential cross section $dN/dt \approx \exp(Bt)$ is shown in Fig. 23b. The averaged value is $\langle B \rangle = 8.42 \pm 0.74$ GeV^{-2}.

In Fig. 23c, the measured total cross sections for the photoproduction of ω mesons by protons are compared with the curve calculated under the assumption of validity of the vector dominance model and the quark model:

$$\sigma(\gamma p \to \omega p) \approx \frac{e^2}{4\gamma_\omega^2}\left(\frac{p_\pi^*}{p_\gamma^*}\right)^2 \exp(-B/t_{\min}) \cdot \times \frac{\sigma(\pi^+ p \to \pi^+ p) + \sigma(\pi^- p \to \pi^- p)}{2}.$$

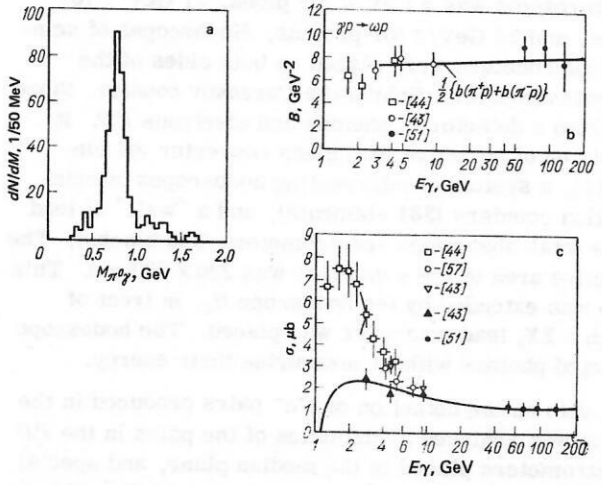

FIG. 23. Mass spectrum of the $\pi^0\gamma$ system[51] (a), energy dependence of the coefficient B for the process $\gamma p \to \omega p$ (b), and total cross sections for photoproduction of ω mesons on protons[51] (c). The curve is calculated in accordance with the vector dominance model and the additive quark model.

In the calculation of the cross sections from the measured quantities, corrections were introduced for the acceptance of the apparatus, the relative probablity of decay B, etc. According to the estimates, the contribution of inelastic events was ≈26% and the systematic error ≈8%.

In Table VI, we give the values of the vector-meson–photon coupling constant determined by the Santa Barbara–Toronto–Fermilab Collaboration[42,51] in their study of the photoproduction of ρ, ω, and ϕ mesons by protons. These values are compared with data obtained with colliding e^+e^- beams and data obtained from the measurement of the A dependence of the photoproduction of vector mesons at lower energies.

These investigations of the photoproduction of vector mesons by protons led to the following conclusions[40,78]:

a) to within the statistical errors, the total cross sections for the photoproduction of ρ and ω mesons are constant in the investigated energy range;

b) the total cross section for the photoproduction of ϕ mesons increases sharply with increasing energy, which may be due to exchange of a pure Pomeron in the t channel;

c) the predictions of the vector dominance model and the quark model agree with the energy dependences of the total cross sections for photoproduction of ρ, ω, and ϕ mesons;

TABLE VI. The vector-meson—photon coupling constants.[51]

Coupling constants	Photoproduction on p (Ref. 78)	A-dependence of photoproduction	Colliding e^+e^- beams
$\gamma_\rho^2/4\pi$	0.65±0.03	0.61±0.03	0.64±0.03
$\gamma_\omega^2/4\pi$	5.4±0.4	7.5±1.3	4.6±0.5
$\gamma_\phi^2/4\pi$	4.7±0.3	5.6±2.4	2.8±0.2

d) the vector-meson–photon coupling constants for ρ and ω mesons obtained from the photoproduction data agree with the values of the constants obtained from the colliding-beam data. However, for the ϕ mesons there is a discrepancy between the values by a factor of about 2.

Photoproduction of ρ^0 mesons was also studied by a P. N. Lebedev Physics Institute–Serpukhov Collaboration at Serpukhov. The arrangement of the experiments is shown in Fig. 24. A beam of electrons with momentum 31 ± 1 GeV/c and a nine-channel combined magnetic and pulse-height tagging system were used.[52] A distinctive feature of this experiment was that measurements were made simultaneously with two targets–liquid hydrogen (0.5 m) and beryllium (0.075 m). Pions from the decay of the ρ^0 mesons were detected in the magnetic spectrometer SIGMA.[53] The particle tracks were measured by blocks of spark chambers with magnetostriction readout. A pulse was fed to the chambers SC_1 and SC_2 in the presence of coincidence of pulses from the tagging system and the counters $S_1 - S_4$ in the absence of a pulse in the total-absorption spectrometer C_{10}. This trigger corresponded to the production of hadrons in the hydrogen target. For the detection of hadron production events in the beryllium target a different trigger was used. In this case, the counter S_4 placed behind the hydrogen target was eliminated and the proportional chamber PC, which was situated behind the beryllium target at a distance of 20 cm, was connected. The results for hydrogen have been published.[54]

Figure 21 shows the total cross section for photoproduction of ρ mesons by hydrogen at energies 15–30 GeV. The data are corrected for events due to target dissociation (8%). It can be seen that the data agree with the results of the other studies and the predictions of the vector dominance model. In Fig. 25, we give the values of the parameters a and b in the expression

$$d\sigma/dt = a \exp(bt).$$

The absence of an energy dependence of $d\sigma/dt\big|_{t=0}$ and the coefficient value $b = 7.5$ (GeV/c)^2 indicate a diffractive nature of the photoproduction of the ρ^0 mesons in this energy range.

Photoproduction of the heavy vector mesons ϕ and $\rho''(1600)$ was studied by a CERN group using the CERN

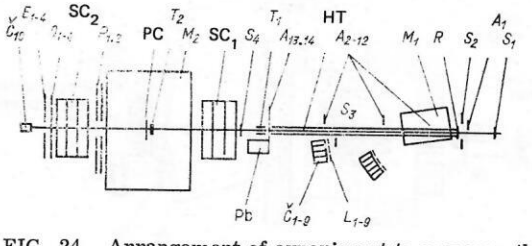

FIG. 24. Arrangement of experiment to measure the photoproduction of ρ^0 mesons (Ref. 54). R is the radiator, S_{1-4}, A_{1-14}, L_{1-9}, $P_{1,2}$, Q_{1-4}, are scintillation counters, C_{1-10} are total-absorption Čerenkov spectrometers, M_1 and M_2 are the tagging magnet and analyzing magnet, HT is the helium tube, Pb is the e-beam absorber, T_1 is the liquid-hydrogen target, T_2 is the beryllium target, SC_1 and SC_2 are spark chambers, and PC is a proportional chamber.

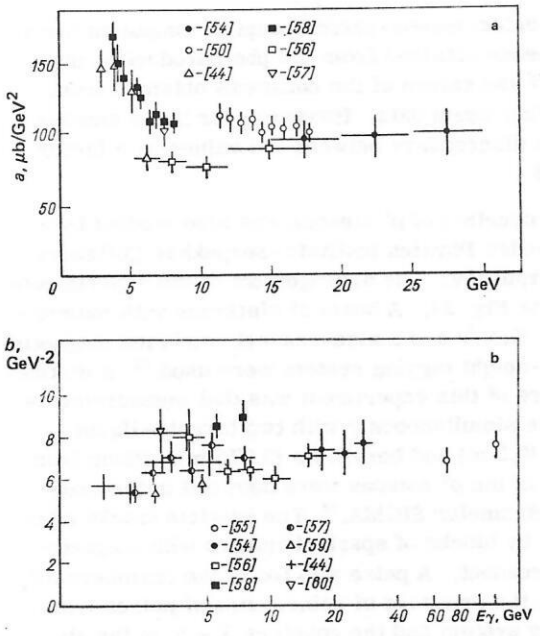

FIG. 25. The parameters a and b in the exponential t dependence of ρ-meson photoproduction.[54]

tagging system and the magnetic spectrometer OMEGA. First results of the investigation were reported at the 1978 Tokyo Symposium[61-63] and later results at the 1979 Batavia Symposium.[64]

The experimental arrangement is shown in Fig. 26. A beam of tagged photons with energies from 20 to 70 GeV was directed onto a liquid-hydrogen cylindrical target of diameter 6 cm and length 67 cm, surrounded by a hodoscope of scintillation counters to detect the recoil protons (24 bantom counters). The target and the main detectors of the charged particles were placed inside a magnet with a field of 0.9T. Behind the target, there was a system of spark chambers (70 gaps) scanned by plumbicons, i.e., there was a television readout. The spark chambers alternated with proportional chambers. Directly behind the magnet there were two drift-chamber modules (four chambers in each), and behind them the hodoscope gas Čerenkov counter C, which was filled with carbon dioxide at atmospheric pressure. The sensitive region of the counter was segmented by 32 photomultipliers. The detection threshold was 5 GeV/c for pions, 17 GeV/c for kaons, and 34 GeV/c for protons. Hodoscopes of scintillation counters were placed on both sides of the Čerenkov counter. Behind the Čerenkov counter, there was also a detector of photons and electrons PD. It consisted of an active lead glass converter (64 elements), a system of intersecting hodoscopes of scintillation counters (384 elements), and a "wall" of lead glass total-absorption spectrometers (340 blocks). The effective area of the γ detector was 280×260 cm. This area was extended by the hodoscope H_3, in front of which a $2X_0$ lead converter was placed. The hodoscope detected photons without measuring their energy.

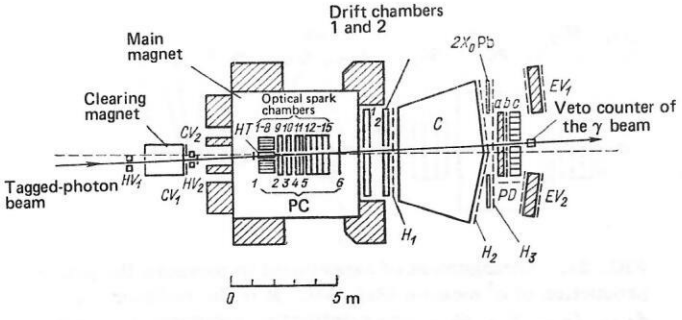

FIG. 26. Schematic arrangement of the facility OMEGA.[61-63] HT is the liquid-hydrogen target, PC are proportional chambers, C is a hodoscope gas Čerenkov counter, H_1—H_3 are hodoscopes of scintillation counters, and the veto counters are collimators.

A veto on the detection of e^+e^- pairs produced in the target was achieved by detection of the pairs in the PD spectrometers placed in the median plane, and special counters EV_1 and EV_2 with filters. Photons that did not interact in the target and multiple bremsstrahlung events were detected by a total-absorption spectrometer placed at the end of the facility.

The photoproduction of ϕ mesons

$$\gamma + p \to \phi + p, \quad \phi \to K^+K^-$$

was investigated[62] by means of a trigger that selected events with two charged particles with large momenta produced in the forward direction in coincidence with a signal from the tagging system and the absence of signals from the Čerenkov counter, the pair veto counter, and the counter of the photons that had not interacted.

As a result of the analysis, 1852 events were selected containing K^+K^- pairs and K^+K^-p triplets, recoil protons with momenta greater than 250 MeV/c being measured. In accordance with the condition of operation of the Čerenkov counter, the photoproduction of K^+K^- pairs was studied in the energy range $20 \leq E_\gamma \leq 35$ GeV of the tagged photons.

The mass spectrum of the K^+K^- mesons is shown in Fig. 27, in which we have also plotted the acceptance curve (broken) calculated by the Monte Carlo method. One can clearly see the peak of the $\phi(1019)$ meson with width 20 MeV, which is determined by the experimental resolution of the apparatus. It was shown that the background of e^+e^-, $\pi^+\pi^-$, and $p\bar{p}$ pairs was negligibly small (1%).

The angular distribution of the $\phi(1019)$ decays with respect to the polar angle in the helicity system is well described by the distribution $\sin^2\theta_{K\Phi}$, which is expected for the decay of a resonance with the quantum numbers $J^P = 1^-$ into a pair of mesons with quantum numbers 0^- provided the s-channel helicity is conserved when this particle is produced.

The dependence of the K^+K^-p events on the momentum transfer can be described by an exponential with the parameters

$$a = 1.18 \pm 0.15 \text{ mb} \cdot \text{GeV}^{-2}, \quad b = 5.5 \pm 1.2 \text{ GeV}^{-2}.$$

The total cross section for the photoproduction of ϕ mesons by hydrogen in the energy range 20–35 GeV, multiplied by B, is

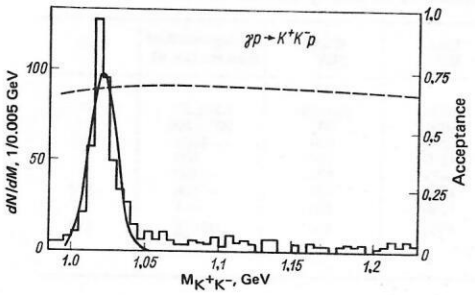

FIG. 27. Mass spectrum of K^+K^- pairs.[62]

$$\sigma(\gamma p \to \phi p)\, B(\phi \to K^+K^-) = 215 \pm 13 \text{ nb},$$

where B is the probability of ϕ decay through the channel $\phi \to K^+K^-$, divided by the total decay probability.

The systematic error is $^{+39}_{-24}$ nb. It is concluded in Ref. 54 on the basis of the analysis of the results that in the investigated interval the total cross section is constant with varying energy to within the error ±10%. Using the tabulated[65] value $B = 0.486 \pm 0.012$, the total cross section

$$\sigma_t(\gamma p \to \phi p) = 442 \pm 29 \text{ nb},$$

is shown in Fig. 22a. It can be seen that the accurate measurement of $\sigma_t(\gamma p \to \phi p)$ is in excellent agreement with the data of other studies and the theoretical curve.

For the study of the photoproduction of ρ'' mesons, the trigger selected hadron events with multiplicity ≥ 4 of the charged particles in the final state.[63] The channel

$$\gamma p \to p\pi^+\pi^-\pi^+\pi^- \qquad (5)$$

was selected by requiring the energy of the initial photon to be equal to the total energy of the four pions ($E_\gamma - \Sigma E_\pi \leq 1$ GeV). In addition, five-track events were added if they had a positively charged particle with momentum less than 1 GeV/c. This track was attributed to the recoil proton. From 1.2×10^6 triggers, 4200 events were selected that satisfied these conditions.

Figure 28 shows the mass spectra of the 4π events for all momentum transfers and also for the interval $0 < -t < 0.3$ GeV^2. In both spectra, there is a peak with center at 1.5 (GeV/c)^2 and FWHM ≈ 0.5 (GeV/c)^2. In Ref. 55, this peak is identified with the $\rho''(1500)$ meson.

Description of the t dependence by an exponential yielded the value $b = 5.1 \pm 0.1$ GeV^{-2} for the slope parameter.

The distribution with respect to the mass of the two pions of the channel (5), which is shown in Fig. 29a, reveals a peak of ρ^0 mesons (in approximately half the cases). The spectrum of the two-pion masses remaining after the subtraction of the ρ meson from the four pions of channel (5) has no ρ^0 peak, i.e., one does not see $\rho^0\rho^0$ decay, which could be expected for a particle with $C = -1$.

Study of the angular distribution of the decays in the helicity system showed that for $M_{4\pi} < 1.8$ (GeV/c)^2 the distribution with respect to the angle θ_{tt} between the sum of the 3-momenta of the two π mesons and the direction of the recoil proton in the rest frame of the four pions corresponds to $\sin^2\theta_{tt}$ and, thus, to a particle with quantum numbers $J^P = 1^-$ and conservation of s-channel helicity when it is produced. At mass $M_{4\pi} > 1.8$ (GeV/c)^2, the background $\cos^2\theta_{tt}$ distribution is dominant. Allowance for the contribution of a particle with quantum numbers 1^- by the method of maximal likelihood yielded the mass spectrum of the four mesons shown in Fig. 28.

It is concluded in Ref. 63 on the basis of the results of the measurements that in the channel $\gamma p \to p\pi^+\pi^-\pi^+\pi^-$ peripheral production of the 4π system with mass ≈ 1.5 GeV and FWHM ≈ 0.5 (GeV/c)^2 is dominant. There is no structure in this peak. The system decays preferentially through the channel $\rho\pi\pi$ and is consistent with the assumption that this is the $\rho''(1600)$ meson with quantum numbers $J^P = 1^-$.

The same group[64] studied the reaction $\gamma p \to \pi^+\pi^- p$. The measured mass spectrum of the 2π system is shown in Fig. 30. One can clearly see a peak corresponding to a particle with mass $M = 1.59 \pm 0.02$ GeV. The width of the peak is $\Gamma = 0.230 \pm 0.08$ GeV. The total cross section for the production of this particle, which is identi-

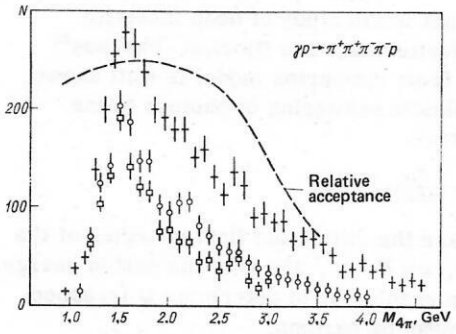

FIG. 28. Mass spectrum of 4π system in the case of photoproduction on hydrogen.[63] The crosses show the mass spectrum of the 4π system with allowance for all values of the momentum transfer; the open circles are with allowance for momenta in the interval $0 < -t < 0.3$ GeV^2, and the open squares with allowance for momenta in the interval $0 < -t < 0.3$ GeV^2 and the contribution of the particle with quantum numbers 1^-.

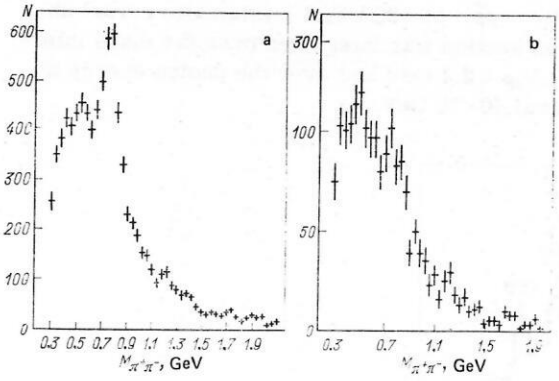

FIG. 29. Mass spectrum of $\pi^+\pi^-$ pairs produced in $\pi^+\pi^-\pi^+\pi^- p$ photoproduction[63] (a) and the mass spectrum of the two pions remaining after the subtraction of the ρ meson from the four pions of the process $\gamma p \to p\pi^+\pi^+\pi^-\pi^-$ (b).

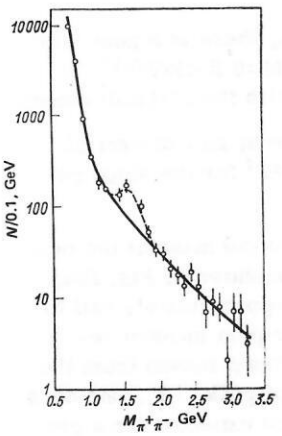

FIG. 30. Mass spectrum of $\pi^+\pi^-$ pairs.[64]

fied as the $\rho''(1600)$ meson in Ref. 79, is 130 ± 20 nb. The branching ratio of the decay channels for the ρ'' meson is

$$\Gamma(\rho'' \to 2\pi)/\Gamma(\rho'' \to 4\pi) = 16 \pm 5\%.$$

As in Ref. 40, one again observes a difference (by a factor two) between the widths of the peaks for the 2π and 4π systems corresponding to the same vector particle with mass $M = 1.6$ GeV. At the present time, the reasons for this discrepancy are not clear.

In Ref. 64, the processes $\gamma p \to \pi^-\pi^-\pi^0\pi^0 p$, $\gamma p \to \pi^+\pi^-\pi^+\pi^-\pi^+\pi^- p$, $\gamma p \to \pi^+\pi^-\pi^+\pi^-\pi^0 p$, $\gamma p \to \pi^+\pi^-\pi^0 p$ (for masses $M > M_\omega$), and $\gamma p \to K^+K^- p$, $\gamma p \to K^+K^-\pi^+\pi^- p$ were also considered. Figure 31 shows the $\pi^+\pi^-\pi^0$ mass spectrum. One can clearly see peaks at the masses 1.275 and 1.675 GeV. In the K^+K^- mass spectrum studied in the process $\gamma p \to K^+K^- p$ ($M > M_\phi$) a peak was observed at $M_{K^+K^-} = 1.76 \pm 0.01$ GeV. The results of the investigation into the heavy vector mesons by the OMEGA group[64] are summarized in Table VII. Eight resonances of the families ρ, ω, and ϕ were observed, and the masses, widths, and total cross sections for photoproduction of them by protons were determined. In some cases, the quantum numbers J^P were determined.

In addition, in the study of the two-particle states in Ref. 64 there were observed for the first time 37 cases of the reaction $\gamma p \to p\bar{p}p$. Estimates were made of the pair-production cross section at mean mass $M_{p\bar{p}} \approx 2.1$ GeV: $\sigma(\gamma p \to p\bar{p} + p) = 20 \pm 4 \pm 6$ (systematic error) nb. The cross section was integrated over the mass interval $1.8 < M_{p\bar{p}} < 2.4$ GeV and over the photon energy in the interval 40–70 GeV.

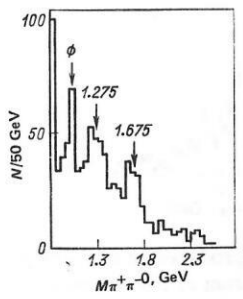

FIG. 31. The $\pi^+\pi^-\pi^0$ mass spectrum, $M > M_\omega$.[64]

TABLE VII. Properties of heavy vector mesons.[64]

Decay channel	Mass, MeV	Width, MeV	Photoproduction cross section, nb	J^P
$\pi^+\pi^-$	1600	230 ± 80	130 ± 20	1^-
$\rho^0\pi^+\pi^-$	1600	500	800 ± 300	1^-
$\omega\pi^0$	1250	300	~ 1000	1^-?
$\pi^+\pi^-\pi^0$	1275	100	~ 100	?
$\pi^+\pi^-\pi^0$	1675	100	~ 100	?
$\omega\pi^+\pi^-$	1700	500	~ 100	1^-?
K^+K^-	1750	100	~ 1	?
$K^*K\pi \to$ $\to K^+K^-\pi^-\pi^-$	1900	400	06^{+30}_{-20}	1^-?

Summarizing, we can say that the investigations made in recent years into the photoproduction of vector mesons in the new energy range (above 20 GeV) have again confirmed the hadronic structure of photons and have led to the discovery of ρ, ω, and ϕ recurrences. Further systematic measurements of these processes are important for obtaining more accurate information about the similarity between hadrons and photons and about the mass spectrum of the vector mesons.

4. COMPTON SCATTERING OF PHOTONS

Closely related to the photoproduction of vector mesons is the elastic scattering of photons: $\gamma + p \to \gamma + p$.

For energies up to 20 GeV and small $t \ll 1$ GeV/c, this process has a diffractive nature: The total cross section depends weakly on the energy and the differential cross section has the exponential form

$$d\sigma/dt = a \exp(bt).$$

The vector dominance model yields a relationship between the cross section of this process and the cross sections for the photoproduction of vector mesons:

$$\frac{d\sigma}{dt}(\gamma p \to \gamma p) = \sum_V (\gamma p \to V_\perp p)\, g_V^2,$$

where $V_\perp$ denotes a transversely polarized vector meson. This relationship is not satisfied when allowance is made for only the ρ, ω, and ϕ mesons. One of the reasons is the possible presence of fixed poles in the amplitude of the process $\gamma p \to \gamma p$. It is therefore important to measure the cross section of this process at high energies, since possible nondiffractive contributions must be strongly reduced in this case.

No less important is the study of deep inelastic photon–nucleon scattering. The Bjorken–Paschos[66] relation deduced from the parton model is well known; it relates the inelastic scattering of photons to the scattering of leptons:

$$\frac{d^2\sigma}{d\Omega\, dE'}\bigg|_{\gamma p} = \frac{\nu^2}{EE'}\frac{d^2\sigma}{d\Omega\, dE'}\bigg|_{ep}\frac{\langle Q^1\rangle}{\langle Q^2\rangle},$$

where E and E' are the initial and final energies of the incident particle, $\nu = E - E'$, and Q is the parton charge. This relationship enables us to determine Q irrespective of what we mean by partons.

An experiment that studies the Compton scattering of photons (elastic and inelastic) in a beam of tagged photons in the range of energies up to 200 GeV is currently nearing completion at Batavia (Heusch *et al.*).

The process $\gamma + p \to \gamma + p + \ldots$ was studied with simul-

taneous detection of the photons in a forward sectioned Pb-lucite total-absorption spectrometer[67,68] and the protons in a recoil detector surrounding the target. The measurements are currently being completed and the data evaluated.

5. PHOTOPRODUCTION OF CHARMED PARTICLES

Photoproduction of the $J/\psi(3100)$ particle was observed for the first time by the Columbia–Hawaii–Cornell–Illinois–Fermilab Collaboration[3] at Batavia; they used the broad-band photon beam produced by 300-GeV protons in a beryllium target (30.5 cm). The arrangement of the experiment is shown in Fig. 16.

The two-muon decay channel

$$\gamma + \mathrm{Be} \to J/\psi + \ldots \\ \qquad\qquad \hookrightarrow \mu^+\mu^-$$

was studied.

The "gray" mass spectrum for events with momentum p_γ greater than 80 GeV/c is shown in Fig. 32. The spectrum shows a background, which increases steadily with decreasing $M_{\mu\mu}$ and is due to the Bethe–Heitler process, and a peak in the region of $M_{\mu\mu} \approx 3.1$ GeV, which contains 60 events. The peak width agrees with the energy resolution of the apparatus.

Figure 33 shows the distribution of the product $B_{\mu\mu} d\sigma/dt_\perp$ with respect to the momentum transfer t events in the region of the 3.1 resonance. The distribution can be described by a sum of two exponentials. One, with slope 50 (GeV/c)^2, characterizes coherent photoproduction on the carbon nucleus, and the other, with slope ≈ 2 (GeV/c)^2, photoproduction on individual beryllium nucleons. It is shown in Ref. 3 that the background from the admixture of neutrons in the beam can be ignored. The upper limit of the background from the admixture of neutrons in the beam can be ignored. The upper limit of the background from the production of $\psi(3700)$ with subsequent decay to the state $J/\psi(310)$:

$$\gamma + \mathrm{Be} \to \psi^1(3700) + \ldots \\ \qquad\qquad \hookrightarrow J/\psi(3100) + \pi^+ + \pi^- \\ \qquad\qquad\qquad\quad \hookrightarrow \mu^+\mu^-$$

is estimated at 15% from the observation of two such events.

From observation of J/ψ events at energy $E_\gamma = 50$–210 GeV, $\langle E_\gamma \rangle = 116$ GeV, the cross section

$$\sigma(\gamma + \mathrm{Be} \to J/\psi)\, B_{\mu\mu}(J/\psi \to 2\mu) = 20 \pm 5 \text{ nb/nucleus}$$

was estimated in Ref. 3. The cross section for production on the nucleon was determined from the differential cross section:

$$\frac{d\sigma}{dt}(\gamma + \mathrm{Be} \to J/\psi + \ldots)|_{t=0}: \\ \frac{d\sigma}{dt}(\gamma + N \to \psi + \ldots)|_{t=0} = 56 \pm 19 \text{ nb/GeV}^2.$$

Under the assumption of validity of the vector dominance model and a purely imaginary nature of the ψN forward scattering amplitude [$\Gamma(\psi \to 2\mu) = 6$ keV, $B_{\mu\mu} = 0.07$],

$$\sigma(\psi N) \approx 1 \text{ mb}.$$

From this it is concluded that the $J/\psi(3100)$ particle is a hadron.

Study of the $J/\psi(3100) \to e^+e^-$ decay channel in this experiment led to determination of the cross section[69]

$$\frac{d\sigma}{dt}(\gamma + N \to J/\psi + \ldots)|_{t=0} = 59 \pm 15 \text{ nb/GeV}^2.$$

The photoproduction of pairs of heavy leptons was also studied in Ref. 3. Cases of two tracks with one corresponding to a muon and the other to an electron were selected. The lower limit of γ-ray detection was 1 GeV. A single event was observed and used to obtain a bound:

$$\sigma(\gamma + \mathrm{Be} \to e^\pm + \mu^\mp + n\gamma + \ldots)\,\varepsilon < 6 \cdot 10^{-34} \text{ cm}^2/\text{nucleus}$$

in which ε includes the geometrical acceptance of the spectrometer for muons and electrons. Under the assumption of 20% B for the leptonic decay channels of the heavy leptons, this value agrees with Tsai's theoretical estimate[37] for $M_{L^\pm} = 2$ GeV and $E_\gamma = 100$ GeV:

$$\sigma(\gamma + \mathrm{Be} \to L^+L^- + \ldots) = 3.3 \cdot 10^{-34} \text{ cm}^2/\text{nucleus}.$$

In a second experiment made with the Fermilab proton accelerator by a Fermilab–P. N. Lebedev Physics Institute–Santa Barbara–Toronto Collaboration,[70] the photoproduction of $J/\psi(3100)$ by deuterium was studied. This used a beam of tagged photons produced by a beam of electrons with energy 90 ± 2 GeV in a copper radiator. The photoproduction of $J/\psi(3100)$ was studied through detection of the $J/\psi \to e^+e^-$ decay mode.

The photon beam was incident on a deuterium target of length 1 m. The paths of the electrons were determined in nine proportional chambers. The electrons

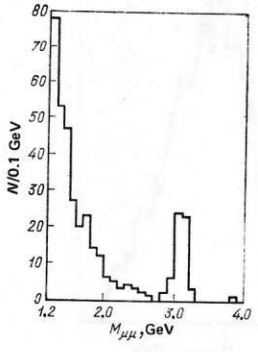

FIG. 32. Spectrum of the masses of muon pairs higher than 1.2 GeV in the case of photoproduction on beryllium.[3]

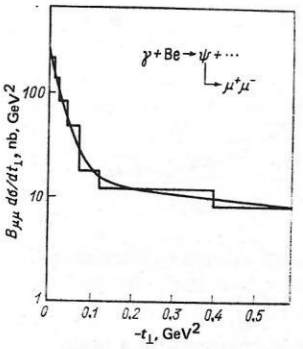

FIG. 33. Dependence of $B_{\mu\mu} d\sigma/dt_\perp$ on t; $B_{\mu\mu}$ is the relative probability of the decay $J/\varphi \to 2\mu$.

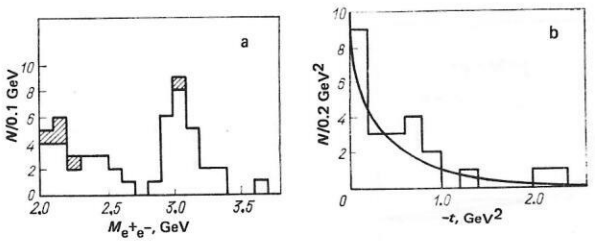

FIG. 34. Mass spectrum of e^+e^- pairs (a) and t distribution of e^+e^- pairs with mass $2.6 < M_{2e} < 3.4$ GeV (Ref. 70) (b).

were identified and their energy measured by a hodoscope of lead glass total-absorption counters (48 elements measuring 6.35 × 6.35 × 50 cm). At the center of the hodoscope there was an opening to allow the photon beam to pass through the facility to the total-absorption spectrometer C. The trigger operator when not less than 65% of the energy of the tagged photon was deposited in the spectrometers. The pulses from all the spectrometers were recorded on magnetic tape and were used to measure both the energy of the electron and the coordinates of its entrance into the spectrometer; these were determined from the shower energy deposited in the neighboring spectrometers. Double measurement of the coordinates by the proportional chambers and the spectrometers made it possible to reduce the background considerably.

The measured mass spectrum is shown in Fig. 34a. The peak in the region of 3100 MeV is identified with the $J/\psi(3100)$ particle (25 events). The width of the peak is ±120 MeV and is determined by the energy resolution of the facility. The hatched region corresponds to inelastic events ($E_{e^+e^-} < 0.85E_\gamma$).

In Fig. 34b, we have plotted the t distribution for elastic events; it can be described by the expression $d\sigma/dt = a\exp(bt)$ with slope parameter 1.8 ± 0.4 GeV^{-2}.

The data were corrected for multiple bremsstrahlung, absorption in the target, and the efficiency of the proportional chambers. The cross section for photoproduction of $J/\psi(3100)$ by deuterium was found to be 80 ± 17 nb. The cross section for the photoproduction of J/ψ by the nucleon was determined from this value, screening being ignored:

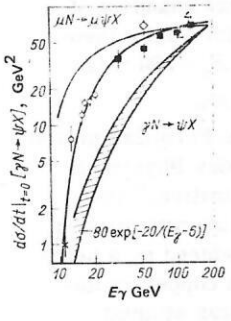

FIG. 35. Energy dependence of the differential cross section of $J/\psi(3100)$ photoproduction on protons. The data are as follows: open triangles, Refs. 3 and 69; open diamonds, Ref. 70; squares, Ref. 72; open circles, Ref. 71; black squares, Ref. 73.

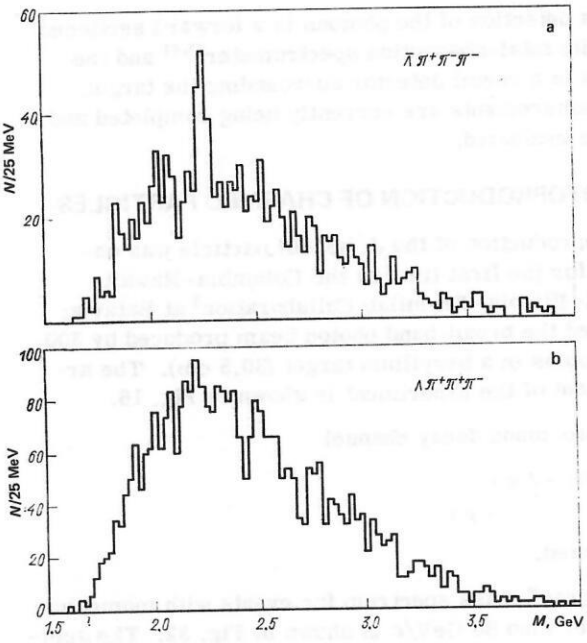

FIG. 36. Mass spectra for $\bar{\Lambda}\pi^+\pi^-\pi^-$ (a) and $\Lambda\pi^+\pi^+\pi^-$ (b).[74]

$$\left.\frac{d\sigma}{dt}\right|_{t=0}(\gamma + N \to J/\psi + \ldots) = 68 \pm 19 \text{ nb/GeV}^{-2},$$

with $\sigma(\gamma + N \to J/\psi + \ldots) = (37.5 \pm 8.2) \pm 4$ (systematic) nb at the mean photon energy 55 GeV.

In Fig. 35, the obtained result is compared with the data of other investigations (Refs. 3, 69, 71, and 72) into photoproduction and the data on the production of J/ψ particles by μ mesons.[73] It can be seen that there is a sharp rise in the cross section in the region of energies from 20 to 55 GeV.

The first results from the study of photoproduction of particles with open charm were reported by the Columbia–Hawaii–Illinois–Fermilab Collaboration, which made investigations with the broad-band photon beam.[3,74] In the study of the $\bar{\Lambda}\pi^+\pi^-\pi^-$ and $\Lambda\pi^+\pi^+\pi^-$ mass spectra (Fig. 36) a peak (60 events) was found in the first spectrum with mass 2.26 ± 0.01 GeV and width 40 ± 20 MeV, the latter being determined by the resolution. The peak was ascribed to the charmed baryon $\Lambda_c(2260)$. In addition, a peak with mass 2.5 GeV was

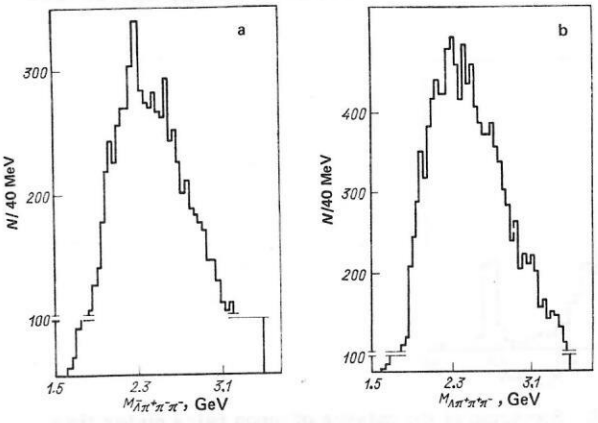

FIG. 37. Mass spectra for $\bar{\Lambda}\pi^+\pi^-\pi^-$ (a) and $\Lambda\pi^+\pi^+\pi^-$ (b).[75]

observed in the five-particle $\bar{\Lambda}(4\pi)^0$ mass spectrum, the peak subsequently decaying in a cascade to $\Lambda_c\pi$.

In a subsequent investigation by the same group with the Fermilab broad-band beam and a CH target, the existence of $\Lambda_c(2260)$ was confirmed.[75] The $\bar{\Lambda}\pi^+\pi^-\pi^-$ mass spectrum again revealed a peak at $M=2.26$ GeV (Fig. 37). As before,[64] no peak was observed in the $\Lambda\pi^+\pi^+\pi^-$ mass spectrum. In addition, some structure was observed in the $\bar{\Lambda}\pi^+\pi^-\pi^-$ mass spectrum in the region of 2.26 GeV. A similar structure was also observed in verification experiments with K^0 mesons, an admixture of which is present in the broad-band photon beam.

These data are in strong disagreement with the results of the OMEGA group at CERN, who did not find any peaks in the mass spectra in their study of $\bar{\Lambda}\pi^+\pi^-\pi^-$ and $\Lambda\pi^+\pi^+\pi^-$ photoproduction.[76,77] It should be noted that in these experiments a beam of tagged photons, in which the admixture of hadrons is much less than in the broad-band beam, was used.

Thus, the existing data on the photoproduction of the charmed baryon $\Lambda_c(2260)$ with decay through the mode $\bar{\Lambda}\pi^+\pi^-\pi^-$ are contradictory, and new measurements are needed to settle this question.

In 1979, detection of photoproduction of the charmed mesons D and F was reported in Refs. 40, 64, 78, and 79.

A group at CERN headed by Diambrini-Pallazi (Bologna–CERN–Florence–P. N. Lebedev Physics Institute–Paris–Santander–Valencia Collaboration) irradiated a photographic emulsion with a beam of tagged photons to look for decays of short-lived particles.[79] The facility OMEGA (see Fig. 26) was used to indicate the search positions of the vertices in the emulsions. The problem of the electromagnetic background was solved ingeniously. The emulsions were placed by means of a tube conveyor in a definite position, exposed to a dose of $\sim 2\times 10^6$ photons, and then replaced. Examination revealed the event shown in Fig. 38, which was interpreted as photoproduction of the D^0 meson. The mass of the particle, which decayed into four charged particles in a time 2.26×10^{-14} sec, was estimated at 1.866 ± 0.008 GeV. The energy of the initial tagged photon was 64.3 GeV. The model-independent estimate of the cross section for photoproduction of

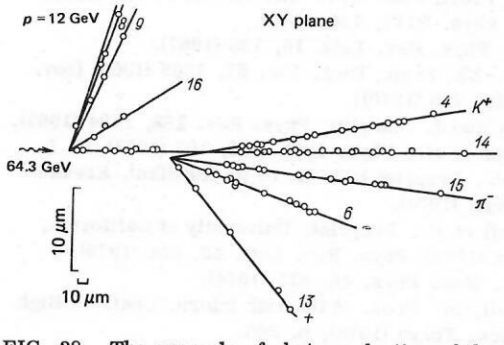

FIG. 38. The example of photoproduction of the D meson observed in a photographic emulsion.[64,79]

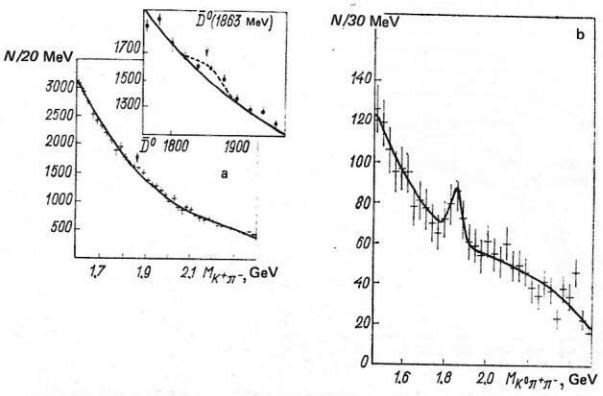

FIG. 39. Mass spectrum for $K^+\pi^-$ (a) and $K^0\pi^+\pi^-$ (b).[64]

charm given by this group is larger than 500 nb. This is the clearest observed case of photoproduction of the D meson.

Searches for the photoproduction of charmed mesons were also made by the OMEGA group.[61,64] The trigger operated only in the case of high multiplicity (≥ 4). The resolution of the facility with respect to the mass of the D meson for the channels $D\to K\pi$ and $D\to K\pi\pi$ was 76 MeV. The preliminary data reported at the Tokyo Symposium[53] in 1978 did not contain any indications of a peak in the $K^\pm\pi^\mp$ and $K^\pm\pi^\mp\pi^\mp$ mass spectra in the region of 1.85 GeV. The data presented a year later at the Batavia Symposium in 1979 revealed peaks corresponding to the D meson in the two decay modes $\bar{D}^0\to K^+\pi^-$ and $\bar{D}^0\to K^0\pi^+\pi^-$ at the mass values 1.863 and 1.862 $\pm$ 0.013 GeV. This can be seen in Fig. 39. Peaks corresponding to the F meson are also observed for the two decay modes $F\to\eta 3\pi$ and $F\to\eta 5\pi$ at the masses $M=2.02\pm 0.07$ and 2.017 ± 0.11 GeV.

The results of the investigation into the photoproduction of charmed mesons obtained by the OMEGA group are summarized in Table VIII.

The same investigation found an excess of direct electrons (positrons) and obtained the ratio $e/\pi\approx 5\times 10^{-4}$, which is appreciably greater than the value 10^{-4} characteristic for processes initiated by hadrons.

Simultaneously with the OMEGA discovery, photoproduction of charmed mesons was observed by a group

TABLE VIII. Summary of results obtained from investigation into the photoproduction of charmed mesons.[64]

Channel	$B\sigma$, nb	B, %	σ, nb
Inclusive e	80 ± 20	10	300 ± 200
$\bar{D}^0\to K^+\pi^-$	5 ± 2	2 ± 0.5	250 ± 100
$D^0\to K^0\pi^+\pi^-$	25^{+16}_{-8}	4 ± 1.3	600^{+400}_{-200}
		2 ± 0.8	1200^{+800}_{-400}
$D^0\to K^-\pi^+$	<7	2 ± 0.5	350
$D^+\to K^\pm\pi^\pm\pi^\pm$	<15	3 ± 0.8	500
$F\to\eta 3\pi$	30^{+20}_{-10}	10 (?)	300^{+200}_{-100}
$F\to\eta 5\pi$	10^{+7}_{-3}	?	—
$F\to\eta\pi$	<5	?	—
$F\to\phi\pi$	<20	?	—

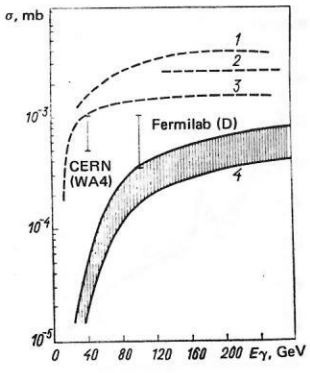

FIG. 40. Estimates of the cross sections of charmed particles.[64] 1) In accordance with the quark fusion model; 2) in accordance with the generalized vector dominance model; 3) in accordance with naive quantum chromodynamics with allowance for unitarity; 4) in accordance with the bag model and gluon bremsstrahlung.

working with the Fermilab broad-band beam.[40,78] Peaks corresponding to the photoproduction of D mesons were observed in an investigation of the $D^0 \to K^\pm \pi^\mp$ and $D^0 \to K^\pm \pi^\mp \pi^+ \pi^-$ decay modes. It was found that the photoproduction cross section for D mesons is 520 ± 110 nb and 540 ± 210 nb, respectively. The systematic error was estimated at $\pm 40\%$.

Figure 40 gives estimates of the cross sections for the production of charmed particles obtained by means of various models[64] and the intervals for the cross sections measured at CERN and Batavia.

Thus, three groups have discovered a new phenomenon—photoproduction of charmed mesons. The large cross section of this process (≥ 500 nb) is striking.

CONCLUSIONS

We can shortly expect exceptionally interesting results from the program of "second-generation" experiments with the accelerators at Batavia[80] and CERN[81] on photoproduction with experimental facilities with luminosity 1 nb/h. These experiments are aimed at studying the photoproduction of new particles and the deep inelastic scattering of photons.

Thus, we see that the development of the electron beam in the Serpukhov proton accelerator was the beginning of a new stage of experimental investigations into the electromagnetic interactions of particles in a new range of energies stretching from tens to hundreds of GeV. Important results have already been obtained in this direction and even more important results and new discoveries are to be expected in the near future.

[1]M. A. Markov, Preprint D-577 [in Russian], JINR, Dubna (1960); V. S. Barashenkov and Din chan Syan, At. Energ. 9, 300 (1960).
[2]S. S. Gershtein *etal.*, At. Energ. 35, 181 (1973); 112, 477 (1973).
[3]W. Lee, in: Proc. of the 1975 Intern. Symposium on Lepton and Photon Interactions at High Energies, Stanford (1975), p. 216; B. Knapp *et al.*, Phys. Rev. Lett. 34, 1040 (1975).
[4]C. Halliwell *et al.*, Preprint FN-241, FNAL (1972); P. Davis *et al.*, Appendix 2 to Proposal N25a, FNAL (1974) (unpublished).
[5]D. Newton and W. Galbraith, Preprint CERN/ECFA/72/4, Vol. 1 (1973), p. 1226.
[6]G. Brianti and N. Doble, Report CERN/EA 77-2 (1977).
[7]B. B. Govorkov, Preprint No. 84 [in Russian], P. N. Lebedev Physics Institute, Moscow (1972).
[8]T. Nash, "Status report on the 300 GeV Electron-Tagged Photon Facility at FNAL," Intern. Symposium on Electron and Photon Interactions at High Energies, Bonn (1973).
[9]V. A. Maisheev *et al.*, Preprint OP 76-15 [in Russian], Institute of High Energy Physics, Serpukhov (1976).
[10]T. Amstrong *et al.*, Preprint CERN/SPSC/74-29 (1974).
[11]B. Knapp *et al.*, Proposal 402, FNAL (1975).
[12]C. A. Heusch, Preprint UCSC 76-056 (1976).
[13]G. Diambrini-Palazzi and A. Santroni, in: Proc. of the Tirrenia Meeting on SPS Experimental Use (1974).
[14]V. A. Maisheev *et al.*, Preprint OP79–63 [in Russian], Institute of High Energy Physics, Serpukhov (1979).
[15]N. Cabibbo *et al.*, Phys. Rev. Lett. 9, 270 (1962); Nuovo Cimento 27, 979 (1963).
[16]I. N. Klimenko, V. A. Maisheev, and A. M. Frolov, Preprint OP 78-100 [in Russian], Institute of High Energy Physics, Serpukhov (1978).
[17]G. Daimbrini-Palazzi, E. Menichetti, and A. Santroni, Nucl. Instrum. Methods 126, 369 (1975).
[18]D. Luckey, in: Summer Study FNAL, Vol. 3 (1968), p. 147.
[19]Z. G. T. Guiragossian and R. F. Rand, Nucl. Instrum. Methods 107, 237 (1973).
[20]B. d'Almagne, Preprint CERN/ECFA/72/4, Vol. 1 (1972), p. 245.
[21]D. F. Alferov *et al.*, Pis'ma Zh. Tekh. Fiz. 2, 487 (1976) [Sov. Tekh. Phys. Lett. 2, 191 (1976)].
[22]P. Astbury *et al.*, Preprint CERN/SPSC/78-76 (1978).
[23]T. Sloan, Preprint CERN/ECFA/72/4, Vol. 2 (1973), p.175.
[24]V. P. Agafonov *et al.*, Prib. Tekh. Eksp. No. 5, 47 (1962).
[25]G. L. Bayatyan *et al.*, Preprint EFI-64 [in Russian], Erevan Physics Institute (1974); E. A. Arakelyan *et al.*, Preprint OP 76-15 [in Russian], Institute of High Energy Physics, Serpukhov (1976).
[26]A. S. Belousov *et al.*, Preprint No. 88 [in Russian], P. N. Lebedev Physics Institute, Moscow (1974).
[27]Yu. A. Aleksandrov *et al.*, Preprint No. 31 [in Russian], P. N. Lebedev Physics Institute, Moscow (1979).
[28]A. Silverman, in: Proc. of the 1975 Intern. Symposium on Lepton and Photon Interactions at High Energies, Stanford (1975); T. H. Bauer, R. Spital, and D. R. Yennie, Rev. Mod. Phys. 50, 380 (1978).
[29]A. S. Belousov *et al.*, Dokl. Akad. Nauk SSSR 215, 76 (1974) [Sov. Phys. Dokl. 19, 123 (1975)]; Yad. Fiz. 21, 556 (1975) [Sov. J. Nucl. Phys. 21, 289 (1979)]; Doctoral Dissertation [in Russian], P. N. Lebedev Physics Institute, Moscow (1974).
[30]D. O. Caldwell *et al.*, Phys. Rev. Lett. 40, 1222 (1978); J. P. Cumalat, Ph.D. Thesis, University of California, Santa Barbara (1977).
[31]B. Margolis, FNAL Pub. 77/71-ThY (1977); F. E. Close *et al.*, Nucl. Phys. B117, 134 (1976).
[32]L. Stodolsky, Phys. Rev. Lett. 18, 135 (1967).
[33]V. N. Gribov, Zh. Eksp. Teor. Fiz. 57, 1306 (1969) [Sov. Phys. JETP 30, 709 (1970)].
[34]S. J. Brodsky and J. Pumplin, Phys. Rev. 182, 1794 (1969).
[35]G. L. Bayatyan *et al.*, Phys. Lett. B56, 197 (1975); G. L. Bayatyan *et al.*, Preprint EFI-72/74 [in Russian], Erevan Physics Institute (1974).
[36]D. O. Caldwell *et al.*, Preprint, University of California, Santa Barbara (1978); Phys. Rev. Lett. 42, 553 (1979).
[37]Y. Tsai, Rev. Mod. Phys. 46, 815 (1974).
[38]D. O. Caldwell, in: Proc. of the 19th Intern. Conf. on High Energy Physics, Tokyo (1978), p. 303.
[39]V. A. Karmanov and A. A. Kondratyuk, Pis'ma Zh. Eksp.

Teor. Fiz. 18, 451 (1973) [JETP Lett. 18, 266 (1973)].
[40]M. Gormley, Report at the 1979 Intern. Symposium on Lepton and Photon Interactions at High Energies, Batavia (1979).
[41]D. O. Caldwell, in: Proc. of the 19th Intern. Conf. on High Energy Physics, Tokyo (1978), p. 303.
[42]R. M. Egloff *et al.*, Preprint Fermilab-Pub. 79/34-EXP (1979).
[43]J. Ballam *et al.*, Phys. Rev. D 7, 3150 (1973).
[44]ABBHHM Collaboration (DESY), Phys. Rev. **175**, 1669 (1968).
[45]R. Anderson *et al.*, Phys. Rev. D 1, 27 (1970).
[46]W. R. Francis *et al.*, Phys. Rev. **38**, 633 (1977).
[47]C. Berger *et al.*, Phys. Lett. **B39**, 659 (1972).
[48]H. J. Besch *et al.*, Nucl. Phys. **B70**, 257 (1974).
[49]H. J. Behrend *et al.*, Nucl. Phys. B144, 22 (1978).
[50]W. G. S. Leith, in: Electromagnetic Interactions of Hadrons, Plenum, New York (1978).
[51]A. Eisner, Report at the 1979 Intern. Symposium on Lepton and Photon Interactions at High Energies, Batavia (1979).
[52]Yu. A. Aleksandrov *et al.*, Preprint No. 31 [in Russian], P. N. Lebedev Physics Institute, Moscow (1979).
[53]Yu. M. Antipov *et al.*, Preprint 74-99 [in Russian], Institute of High Energy Physics, Serpukhov (1974).
[54]Yu. A. Aleksandrov *et al.*, Preprint No. 101 [in Russian], P. N. Lebedev Physics Institute, Moscow (1979).
[55]R. Wilson, in: Proc. of the 19th Intern. Conf. on High Energy Physics, Tokyo (1978), p. 306.
[56]J. Park *et al.*, Preprint SLAC-Pub-972 (1971); Nucl. Phys. **B36**, 404 (1972).
[57]Y. Eisenberg *et al.*, Phys. Rev. D 5, 15 (1972).
[58]G. McCellan, Phys. Rev. D 4, 2683 (1971).
[59]J. Ballam *et al.*, Phys. Rev. D 5, 545 (1972).
[60]M. Davier *et al.*, Phys. Rev. D 1, 790 (1970).
[61]A. Kemp, in: Proc. of the 19th Intern. Conf. on High Energy Physics, Tokyo (1978), p. 300.
[62]D. Aston *et al.*, Preprint ASE/B3E/B4E (1978).
[63]D. Aston *et al.*, Preprint B3E/B4E/A5E (1978).
[64]F. Richard, Report at the 1979 Intern. Symposium on Lepton and Photon Interactions at High Energies, Batavia (1979).
[65]Review of Particle Properties, Particle Data Group (1978).
[66]J. D. Bjorken and E. A. Paschos, Phys. Rev. **185**, 1975 (1969).
[67]C. A. Heusch and C. Y. Prescott, Preprint CTSL-41 (1964).
[68]C. A. Heusch *et al.*, in: Mezhdunar konf. po apparature v fizike vysokikh énergiĭ (Intern. Conf. on Instruments in High-Energy Physics), Vol. 1, Dubna (1971), p. 419.
[69]L. R. Cormell, Ph.D. thesis, University of Illinois (1976).
[70]T. Nash *et al.*, Preprint Fermilab-Pub. 76/25 EXP (1976); Phys. Rev. Lett. **21**, 1233 (1976).
[71]B. Gittelman *et al.*, Phys. Rev. Lett. **35**, 1616 (1975).
[72]U. Camerini *et al.*, Phys. Rev. Lett. **35**, 483 (1975).
[73]A. R. Clark *et al.*, Phys. Rev. Lett. **43**, 187 (1979).
[74]W. Y. Lee, in: Proc. of the 1977 Intern. Symposium on Lepton and Photon Interactions, DESY, Hamburg (1977), p. 555.
[75]W. Y. Lee, in: Proc. of the 19th Intern. Conf. on High Energy Physics, Session B4E, Tokyo (1978).
[76]D. Aston *et al.*, in: Proc. of the 19th Intern. Conf. on High Energy Physics, Tokyo (1978), p. 805.
[77]E. Gabathular, in: Proc. of the 19th Intern. Conf. on High Energy Physics, Tokyo (1978), p. 801.
[78]W. W. Lee *et al.*, Phys. Rev. Lett. **43**, 347 (1979).
[79]G. Diambrini-Pallazi, in: Proc. of the 19th Intern. Conf. on High Energy Physics, Tokyo (1978), p. 297.
[80]J. Appel *et al.*, Proposal N 516, FNAL (1976); E. Barsotti *et al.*, FNAL TM-823 (1978).
[81]P. Astbury *et al.*, CERN/SPSC/78-76, SPSC/P-109 (1978).
[82]D. S. Ayres *et al.*, Phys. Rev. D **15**, 3105 (1977).
[83]I. Ambats *et al.*, Phys. Rev. D **9**, 1179 (1974).
[84]D. O. Caldwell *et al.*, Phys. Rev. D 7, 1362 (1973).
[85]V. Heynen *et al.*, Phys. Lett. B34, 651 (1971).
[86]S. Michalovski *et al.*, Phys. Rev. Lett. **39**, 737 (1977).

Translated by Julian B. Barbour